Rolling contact bistable passive and active metamaterials

Mohammad Naghavi Zadeh*, Fabrizio Scarpa, Jonathan Rossiter*

Supplementary Information

SI-1. Metamaterial design details

In this section, the design details of the bistable rolling mechanism are discussed using mathematical modelling and numerical simulations.

SI-1.1. Rotational angle limits

The out of plane width of the strips and the width of the walls are equal to b. However, the walls need to have a limited rotational angle based on the design, therefore, two equal length embossed segments with distance S from the hinge act as stoppers against the constraint (Figure S1). In general, the convergent and divergent section angles can be different, but the constraint profile needs to be modified to address this requirement. Hence, the general configuration of the constraint and wall dimensions are presented in Figure S1. The eccentricity e is half the thickness of the wall, although in general it could be also different for two neighboring cells by avoiding the symmetry where the hinge center is not on the wall's center line.

The dimensions of the constraint can be defined by convergent (θ_c) and divergent angles (θ_d) and the distance S, where two dimensions S_c and S_d are calculated according to Equations S1 and S2.

$$S_c = S.\cos\theta_c \quad \text{S1}$$

$$S_d = S.\cos\theta_d \quad \text{S2}$$

When convergent (θ_c) and divergent angles (θ_d) are equal, then $S_c = S_d$ and the constraint will have a regular rectangular geometry as shown in Figure 1b in the manuscript.

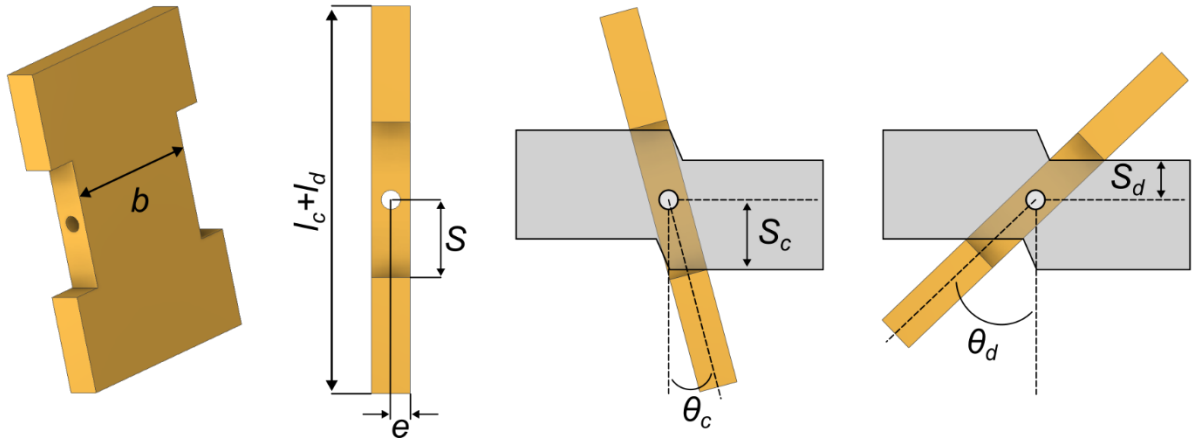

Figure S 1- Dimensions of the wall and the constraint in general case.

SI-1.2. Strip deformation analysis and length estimation

In order to derive the strains and displacements with proper precision, a model or a closed form solution is required to correlate the strip length l_S, the width W, and the angle θ to each other. Due to complex contact conditions and nonlinear deformations of the strip, we have developed an approximate statistical-analytical approach to explore the deformation of the strip, which is the main determinant of the strain capacity and stress analysis at different widths, angles, and strip thicknesses. In this regard, we develop a curve-fitting program in MATLAB, which fits an ellipse to the strip as shown in Figure S2. The strip has a constant length l_S, which can be divided into three sections (Figure S2a): part of the length attached to the rotating wall, l_W, part of the length attached back-to-back to the other strip at the centerline and contributes to rolling, l_R, and part of the length between two tangent contact points of the strip on the wall and the centerline where strip is bent, l_B. In general, the length of the strip is constant, hence, the sum of these three sections should be constant, as shown in Equation S3.

$$l_S = l_W + l_B + l_R \tag{S3}$$

Since the wall lengths (l_C and l_d) are known, selecting a specific point of contact on the wall defines l_W. Now, we have one equation (S3) and two unknowns, which are the rolling length and the bent length. The bending curvature of the strip is a function of elastic response of the strip under certain geometry and boundary conditions at each point in the channel. As deriving this deformed shape from the theory of elasticity is a non-trivial process due to complex boundary conditions at the contact points at two ends of the bent section of the strip, we use statistical analysis to estimate the shape function of the bent section.

As nonlinear deformations of beams typically follow elliptic integrals, we use an ellipse fitting algorithm to fit an ellipse to the bent section of the strip. The purpose of this methodology is to find a relationship between geometrical parameters of the strip/channel (mainly θ) and ellipse parameters such as eccentricity, *ecc*.

SI-1.3. Ellipse Tangency Problem Setup and Solution Summary

This section summarizes the assumptions, derivations, and geometry for an ellipse tangent to a vertical line (representing the centerline between two strips), an inclined line (representing the wall), and in the second case also to a horizontal line, with the major axis aligned along the angle bisector of the two non-parallel lines.

According to Figure S2, we have:

- Vertical line: $x = 0$.
- Inclined line: $y = mx$ (meeting the vertical at the origin).
- Let the major axis of the ellipse lie along the internal angle bisector of $x = 0$ and $y = mx$.

Rotate the plane so the U-axis is that bisector and the V-axis is perpendicular to it. In (U,V)-coordinates the two lines ($x = 0$ and $y = mx$) become a symmetric pair, where every point on the vertical or inclined line in (U,V)-coordinates follows Equation S4.

$$V = \pm \tan(\alpha)\, U \tag{S4}$$

$$\alpha = \frac{1}{2}\left(\frac{\pi}{2} - \arctan\,(m)\right) = \frac{\pi}{4} - \frac{1}{2}\arctan\,(m) \tag{S5}$$

Denote $m' = \tan(\alpha)$ where angle $\alpha = \frac{\pi}{2} - \frac{\theta}{2}$. The ellipse has a long semi-axis a (along U) and a short semi-axis $b = r.a$ (along V), with $r = \sqrt{1 - ecc^2}$ from the given eccentricity ecc. By symmetry, the center of ellipse is on the U-axis as $(U,V) = (C,0)$. Figure S2b-c show the geometric setup with U and V axes:

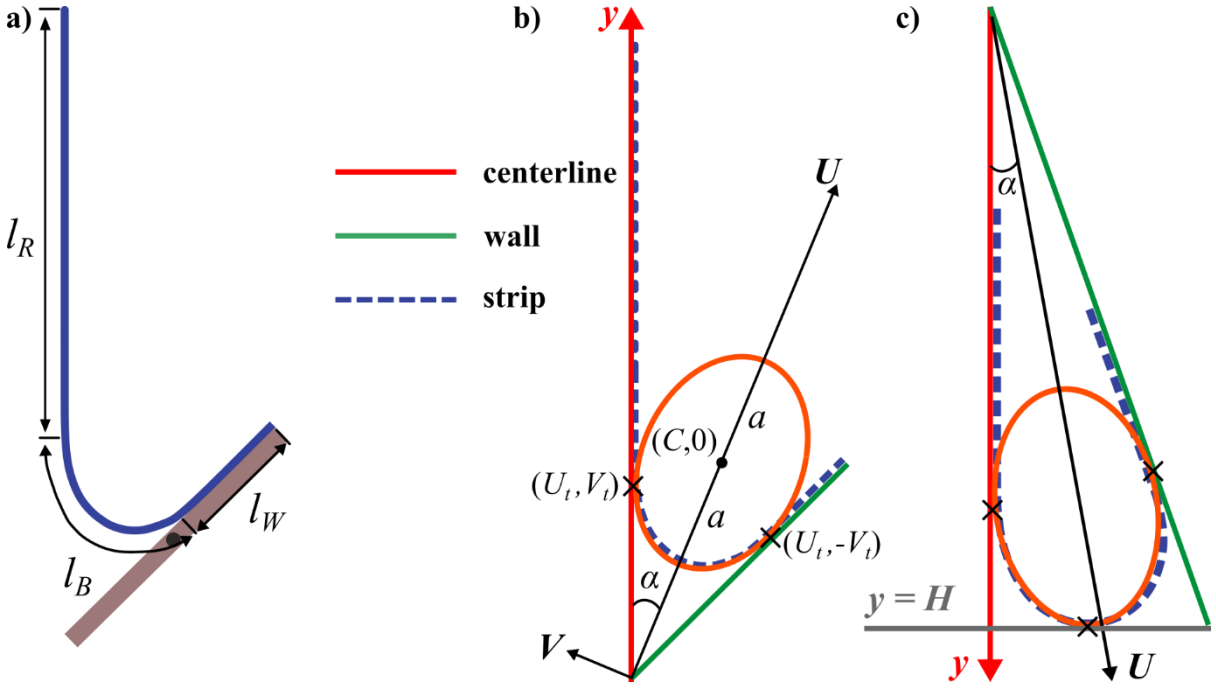

Figure S 2. Strip and ellipse fitting. a) definition and position of different sections along a bent strip, b) coordinate systems and configuration of an ellipse in and ellipse fitting problem in convergent side, and c) in divergent side of the wall.

To apply the ellipse equations later for determining the geometrical parameters of the deformed strip section, two distinct cases are considered. The first case represents the contact point of the strip on the wall being known, *i.e.*, l_W is known and the position of the tangent point on the inclined line is known as a result. The second case includes the presence of a horizontal line that is coincident with the end point of the inclined line (rotating wall) and represents the maximum displacement limit of the strip in a tessellation. It should be noted that both cases are considered for a known value of W and θ, where a known value of specific ecc will be associated to them as discussed in SI-1.4.

Case 1: Tangent point on the inclined line is known

Given the tangency point (U_t, V_t), the center C and semi-major axis a are computed by:

$$C = U_t\left(1 + \frac{m'^2}{r^2}\right) \tag{S6}$$

$$a^2 = {U_t}^2 \frac{m'^2}{r^2}\left(1 + \frac{m'^2}{r^2}\right) \tag{S7}$$

$$b = r\,a \tag{S8}$$

The ellipse equation in the (U,V)-frame is then:

$$\frac{(U-C)^2}{a^2}+\frac{V^2}{b^2}=1 \tag{S9}$$

Case 2: Tangent to three lines: $x = 0$, $y = mx$, and the horizontal $y = H$.

This case provides the methodology to calculate the maximum strain capacity of the bistable mechanism for a given strip length l_S and the wall length ($l_C + l_d$). In the (U,V) frame, tangency to $V = \pm m'U$ and $y = H$ yields:

$$a^2 = \frac{m'^2}{r^2+m'^2}C^2 \tag{S10}$$

$$(H + C\sin\theta)^2 = a^2\sin^2\theta + b^2\cos^2\theta \tag{S11}$$

which solve for C and then a and b. Tangent points on vertical/inclined lines are:

$$U_t = \frac{r^2}{r^2+m'^2}C \tag{S12}$$

$$V_t = \pm m'U_t \tag{S13}$$

Parametrize the ellipse in (U,V):

$$U = C + a\cos t \;\;,\; t \in [0,2\pi)\text{ t} \tag{S14}$$

$$V = b\sin t \tag{S15}$$

To obtain the slope at tangent point, differentiate with respect to t:

$$\frac{dV}{dU}=\frac{dV/dt}{dU/dt}=\frac{b\cos t}{-a\sin t}=-\frac{b}{a}\cot t \tag{S16}$$

Considering the vertical and inclined lines in (U,V)-frame, we have $V = \pm m'U$ and $m' = \tan\alpha$. At tangent points we have:

$$-\frac{b}{a}\cot t = \pm m' \tag{S17}$$

Considering $b = ra$:

$$\tan t = \pm r/m' \tag{S18}$$

Let $\psi = \tan^{-1}(r/m') \in (0,\pi/2)$, then tangency parameters will be $t = \psi$ & $t = \pi - \psi$. The arc length of the ellipse between tangencies on the side closer to $y = H$ is:

$$l_B = \int_{\psi}^{\pi-\psi} \sqrt{a^2\sin^2\theta + b^2\cos^2\theta}\,d\theta = 2a\,E\left(\frac{\pi}{2}-\psi|ecc^2\right) \tag{S19}$$

where $E(\cdot|\cdot)$ is the incomplete elliptic integral of the second kind and *ecc* is eccentricity of the ellipse. Therefore, we need to have the right value for eccentricity *ecc* for a design case to be able to derive the displacements and strains. Equation S19 is also applied to case 1 to calculate the length of the ellipse between the two contact points.

SI-1.4. Statistical analysis of ellipse eccentricity using FEM results

Deriving a closed-form solution and elastica function for this problem is challenging due to the complexity of the contact boundary conditions between the strips. Therefore, we use a statistical approach to interpolate the eccentricity *ecc* of an ellipse for given geometrical parameters of the mechanism. The main geometrical parameters to consider are width W, angle θ, and thickness of the strip t. In this study, we performed multiple finite element simulations (as described in detail in section SI-3) for different models with changing one geometric parameter as a variable, while others remained constant. We found from an initial survey on simulations that eccentricity of the ellipse fitted to the deformed section of the strip, l_B, is mainly dependent on angle θ. We, therefore, performed simulations on a model with t = 0.1 mm, W = 90 mm, and angles θ = [10, 20, 25, 30, 35, 40, 45]. In each simulation, the three length sections of the strip were separated using the contact status data from Abaqus. An example for a case with θ = 25 degrees is shown in Figure S3. Different frames of the deformation are presented with deformed strip (black), range of nodes detected on the bent length and between contact points on the rotating wall and centerline (red) and best fitted ellipse (blue). A path on the edge of the strip was defined in Abaqus and the displacement coordinates and contact status (zero or one) for the nodes on the path were obtained. The ellipse fitting is optimized for the angle ϕ between the ellipse's long semi-axis and the centerline, where the root mean square error (RMSE) of the fitted ellipse is minimized. As ellipse's long semi-axis lies on the bisector line, we can say $\theta = 2\phi$. In the analysis of the specific case shown in Figure S3, the wall starts rotating in frame 72 and stops at frame 109.

The eccentricity of ellipse, *ecc*, is averaged over multiple frames on converging and diverging side and the average values and standard deviation are presented in Table S1. As the simulations are dynamic and the strip has small oscillations during its rolling motion, the angle ϕ and *ecc* have a variance over a range of frame numbers and therefore standard deviation in some cases is large. In order to estimate the *ecc* value for an arbitrary angle, polynomial curve fitting on ecc values at convergent and divergent side is performed. Difference of linear and quadratic curve fitted to data in divergent side is negligible. On the convergent side, there is a slight difference between linear and quadratic fitted lines, however, the RMSE for both cases is very small where $\text{RMSE}_{\text{quad}}$ = 0.0065 and $\text{RMSE}_{\text{linear}}$ = 0.0084. The coefficients of the linear and quadratic equations fitted to convergent and divergent eccentricity data are presented in Table S2. Having this data, one can determine different length sections of the strip by knowing the contact position of the strip on the wall as described in SI-1.3.

Another important observation from FE simulations is that the wall starts rotating once the contact point on the wall reaches the hinge point, which means $l_W = l_C$ and then the contact point position on the wall remains constant during the rotation, while the bent section length l_B and rolling length l_R change. Therefore, we divide the analysis into three parts:

i) Strip converging: stress increases, ellipse's eccentricity (ecc_c) is constant, l_W increasing.

ii) Wall rotating: stress reducing, ellipse's eccentricity changes, l_W is constant.
iii) Strip diverging: stress reducing, ellipse's eccentricity (ecc_d) is constant, l_W increasing.

Therefore, if we divide the motion of the mechanism into three stages of convergent, rotating, and divergent, we know that at the end of the convergent stage, during the rotating stage, and at the beginning of the divergent stage, the position of the contact point of the strip on the wall is known. This helps in determining the position of the stoppers as later discussed and in defining the total length of the strip required to achieve a certain strain as instructed in section SI-1.3.

Table S 1. Eccentricity values obtained from FE simulations for different angles.

	Convergent		Divergent	
Angle θ	*ecc*	Std.	*ecc*	Std.
10	0.709045	0.008661	0.688796	0.005046
20	0.713669	0.004948	0.685714	0.00733
25	0.7298	0.009843	0.6824	0.002879
30	0.737925	0.007666	0.679374	0.001059
35	0.77185	0.026421	0.687536	0.010572
40	0.77587	0.017638	0.685876	0.002738
45	0.789593	0.012088	0.676663	0.000967

Table S 2. Coefficients of the linear and quadratic curves fitted to eccentricity data.

	Convergent			Divergent		
	a	*b*	*c*	*a*	*b*	*c*
Linear ($ax+b$)	0.0025582	0.6719005	-	-0.0002063	0.6898096	-
Quadratic (ax^2+bx+c)	0.0000435	0.0001449	0.6998002	0.0000005	-0.0002354	0.6901453

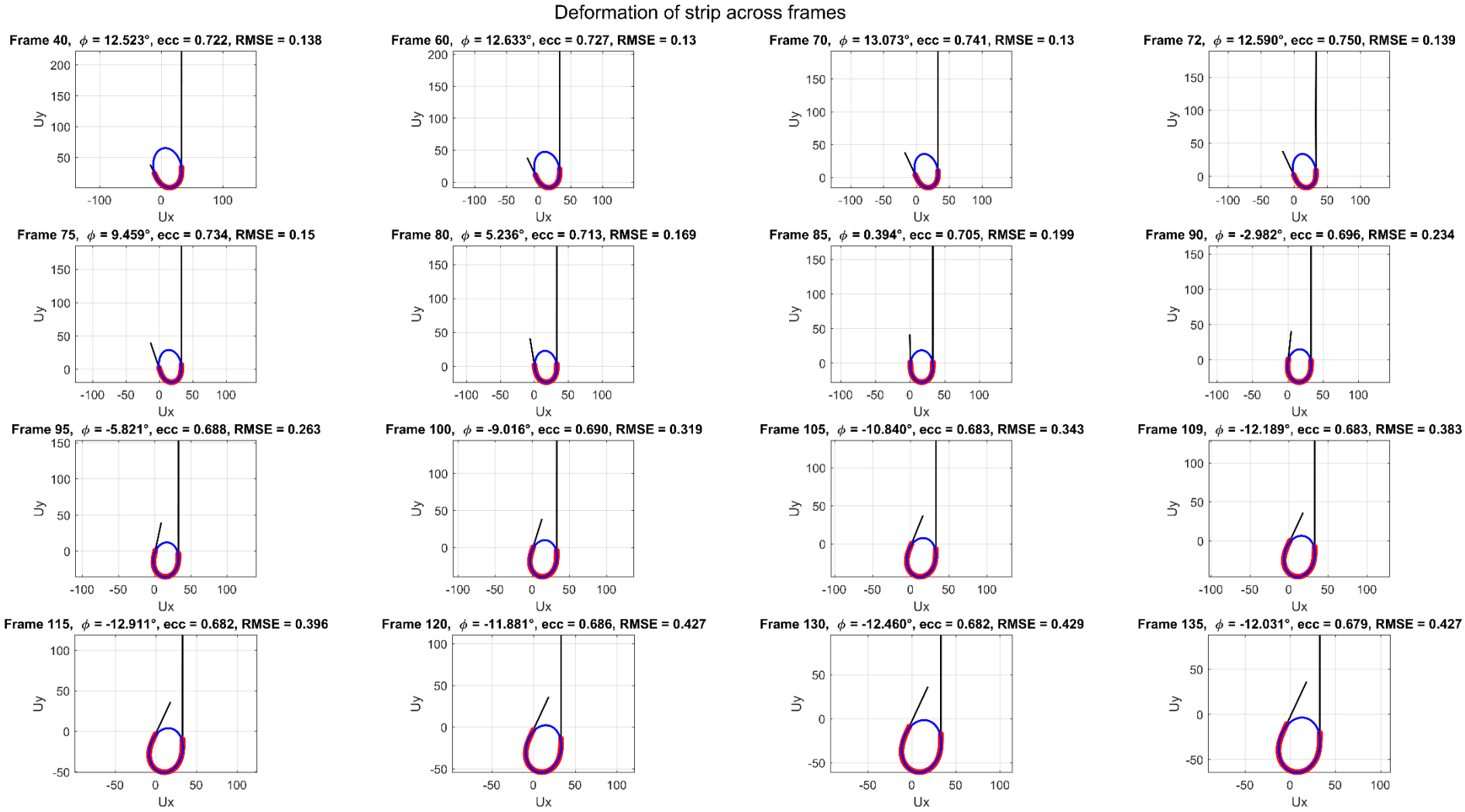

Figure S 3. Different frames from deformation of a strip and ellipse fitting.

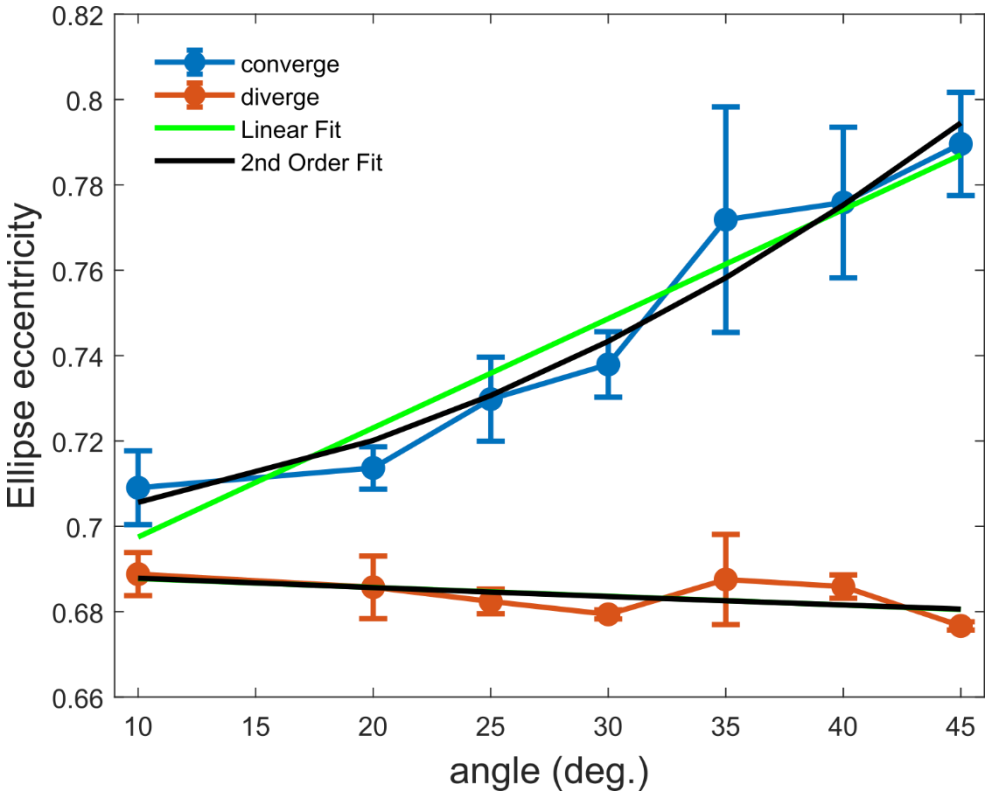

Figure S 4. Eccentricity values obtained by ellipse fitting to strips at different angles and averaged over different frames on convergent and divergent sides of the mechanism.

SI-1.5. Calculating strain and different length sections: inverse problem

Previously in sections SI-1.3 and SI-1.4, the methodology for ellipse fitting was explained and eccentricity values for ellipses were evaluated. In this section, the inverse problem will be solved where the eccentricity of the ellipse (*ecc*) is known and one tangent point (case 1) or one horizontal limit (case 2) is defined. To model the problem, first geometrical references of the problem are parameterized. The rotating wall is parameterized as shown in Figure S5, where the rotation point, P_r, top point of the wall P_T, and bottom point of the wall P_B are defined. The coordinates of these points are:

$$\left(P_r^x, P_r^y\right) = \left(\frac{W}{2}, \frac{W\cos\theta - 2e}{2\sin\theta}\right) \quad \text{S20}$$

$$\left(P_j^x, P_j^y\right) = \left(P_r^x - e\cos\theta\,, P_r^y + e\sin\theta\right) \quad \text{S21}$$

$$\left(P_T^x, P_T^y\right) = \left(P_j^x + l_c\sin\theta\,, P_j^y + l_c\cos\theta\right) \quad \text{S22}$$

$$\left(P_B^x, P_B^y\right) = \left(P_j^x - l_d\sin\theta\,, P_j^y - l_d\cos\theta\right) \quad \text{S23}$$

Once the coordinates of the top point are known, the coordinates of the tangent point on the wall in case 1 can be determined by knowing the l_W. Considering the other two constraints that the long semi-axis is on bisector line and there is a tangent point on x=0 line and knowing the value of the eccentricity, *ecc*, for a given angle θ; it is possible to fit a unique ellipse. For the convergent stage, the shorter arc length between the two tangent points in this ellipse is equal to l_B. For a specific case of θ = 25 degrees and W = 70 mm, the ellipse and tangent points are shown in Figure S6, where short and long arcs are highlighted and their lengths are given. The code used to create this figure is presented in SI-9.1.

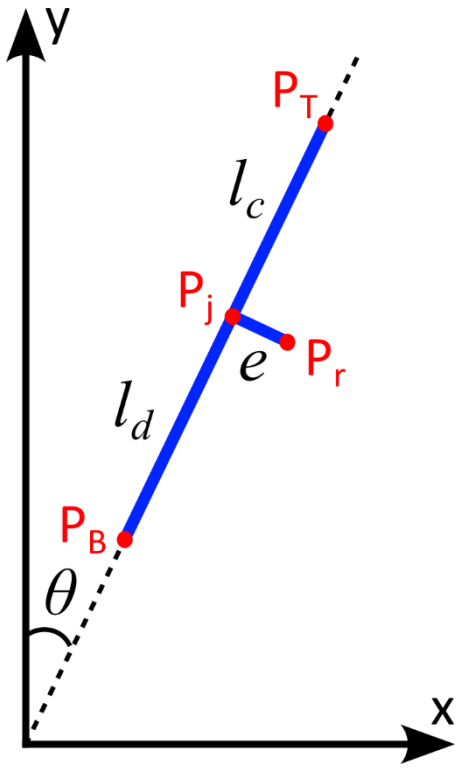

Figure S 5. Parameters of the rotating wall and end point definitions.

For case 2, we assume that the strip displacement limit is when the bent strip touches the horizontal line passing through the bottom point P_B in the divergent stage. In this case, we do not know how much l_W is, but we know the vertical limit is the line $y = P_j^y + l_d \cos\theta$. We use statistical data to find the ellipse eccentricity for a given angle at the divergent side. Hence, we have four constraints including three tangent lines and alignment of long semi-axis with bisector line. Once the ellipse is fitted and the tangent points on the inclined and vertical walls are identified, the values for l_W and l_B in the divergent stage are known, where l_B is the long arc length between two tangent points of the ellipse. Figure S7 illustrates the ellipse fitting for case 2 where tangents on three lines is highlighted.

To find the strain value, first we must define the length of the strip. If length of the strip is not defined, we can find the minimum length of strip using case 2. In this case, we assume that l_c and l_d are known and the l_B and l_W are found using ellipse fitting. We also assume that the free end of the strip has the same y-coordinate as the P_T, which means that in a lattice (as shown in Figure 1e of the manuscript), the strip is totally bound between the horizontal boundaries, where the bent section is tangent to the horizontal line passing through the P_B and the top end of strip intersects the horizontal line passing through the P_T. Hence, $l_R = P_T^y - y_t^{x=0}$ where $y_t^{x=0}$ is the y-coordinate of the tangent point of the ellipse on the line $x = 0$. Therefore, length of strip can be calculated as $l_s = l_R + l_B + l_W$.

Knowing the l_s, we go back to case 1 and find the l_R on the convergent section for $l_W = 0$. Then, we can calculate the value of parameter L (as shown in Figure 1d of the manuscript) from the equation $L = l_R + y_t^{x=0} - P_r^y$, where $y_t^{x=0}$ is the y-coordinate of the tangent point of the ellipse on the line $x = 0$ in case 1. The total rolling displacement of the strip in this case is $\Delta L = l_R + y_t^{x=0} - P_T^y$; hence, strain can be derived from $\varepsilon = \Delta L/L$. This process is presented in the MATLAB code of SI-9.2.

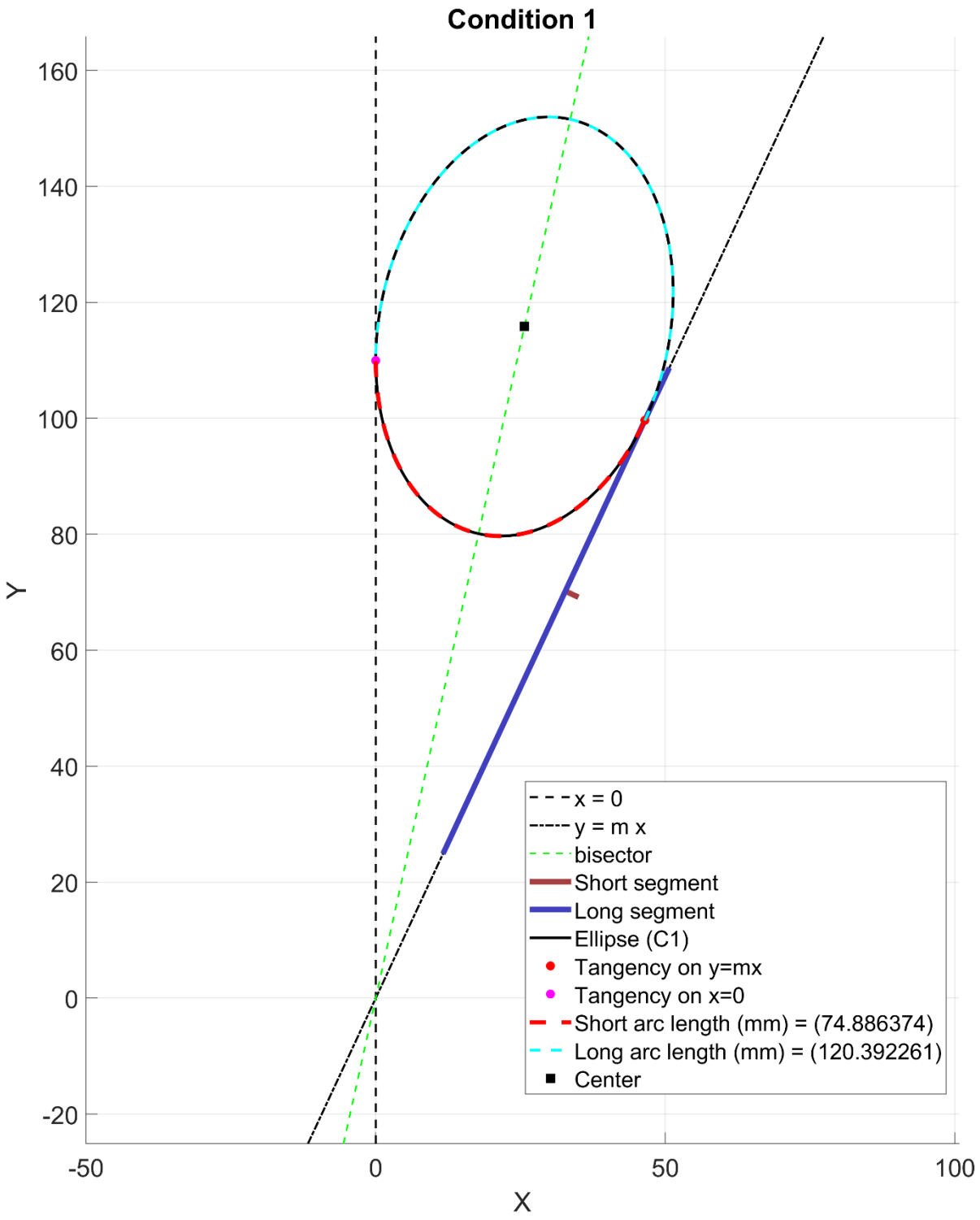

Figure S 6. Ellipse fitted for convergent side using a tangent point, two tangent lines, and angle bisector line as constraints.

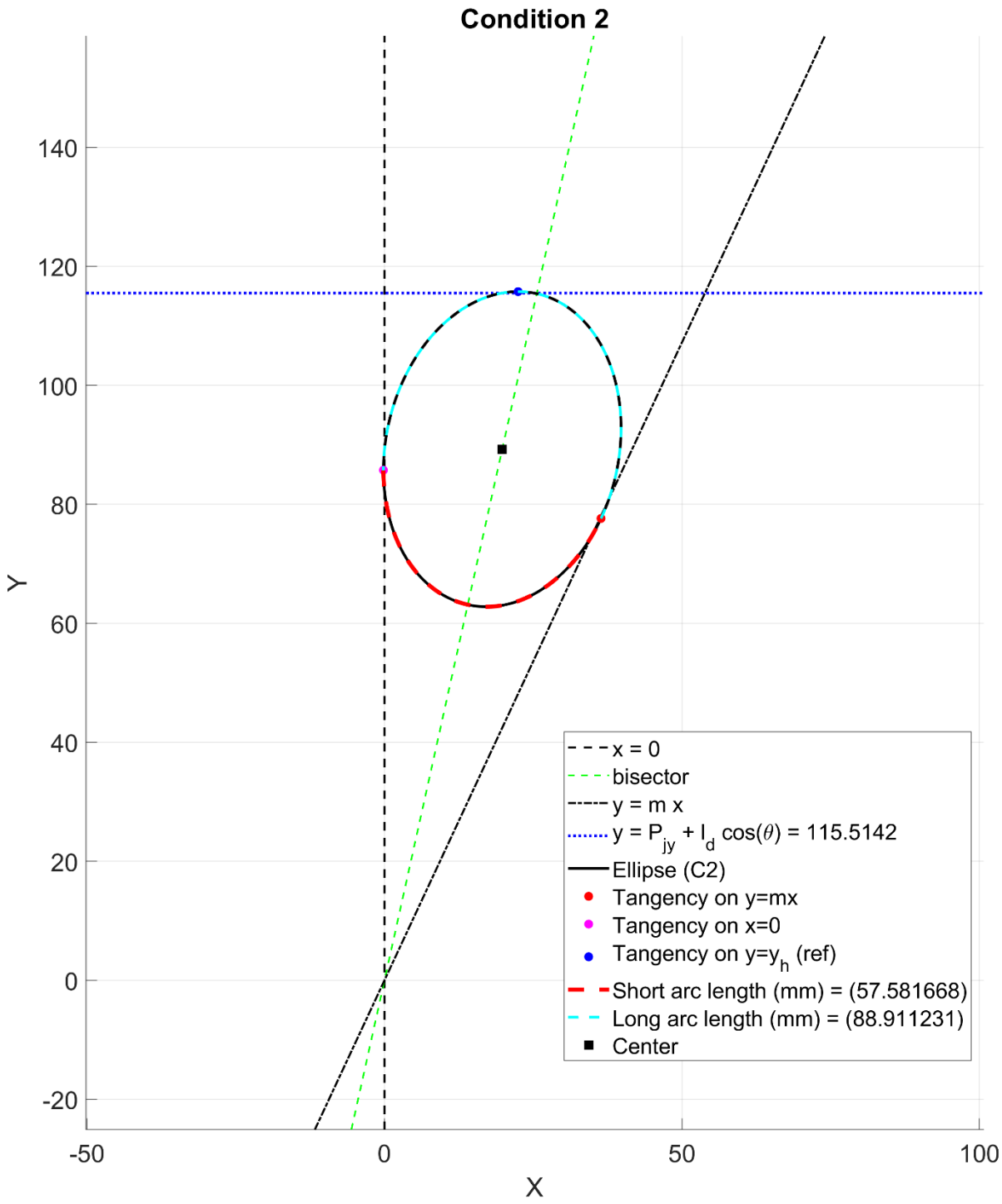

Figure S 7. Ellipse fitted with three tangent lines for case 2 on the divergent side.

SI-1.6. Calculating stress in the strip

The maximum stress in the strip should be calculated to ensure that the chosen material, thickness, and geometrical parameters W and θ are suitable for the bistable mechanism and do not exceed the yield stress. Based on results from SI-1.3 and SI-1.4, the maximum curvature of the strip estimated by an ellipse occurs at the apex of the ellipse, which is on the bisector line. As discussed in the manuscript and shown in Figure 2c(iii), the maximum stress occurs at the end of the convergent stage and beginning of the wall's rotation. We know that at this point,

the strip contact point on the wall is at the closest point to the hinge (on the hinge, if $e = 0$). Once a tangent point of an ellipse and the angle θ and width W are known, an eccentricity ecc for the ellipse can be estimated from SI-1.4, and the ellipse could then be fitted as in case 1 of SI-1.3. Once the ellipse is fitted and the semi-major axis a is known, the minimum radius of curvature can be calculated from Equation S24.

$$\rho_{min} = a\sqrt{1 - ecc^2} \tag{S24}$$

As the maximum stress in the strip occurs at minimum radius of curvature, it can be computed using Equation S25.

$$\sigma_{max} = \frac{Et}{2\rho_{min}} \tag{S25}$$

For a specific case of $W = 70$ mm and $\theta = 25$ deg., the maximum stress obtained from FEM and our ellipse fitting methodology (Equation S25) are 1743 MPa and 1644 MPa, respectively. The relative error is 6.0%, which indicates a good accuracy of the ellipse fitting method in stress estimation. The stress calculation is also implemented in the MATLAB code presented in SI-9.2.

SI-1.7. Buckling analysis

The buckling of the strips is a failure mechanism where the strips fail to roll past the minimum width point of the channel. The critical buckling load in this mechanism depends on the rolling length, l_R, the width of the channel W, the angle θ, and the boundary conditions of the strip at the top and bottom. One challenge in studying the buckling critical load in this case is the contact between the strips at the rolling point, where boundary conditions are not perfectly pinned or clamped. In addition, a random trend is observed in the buckling mode shape of the strips in experiments indicating sensitivity to the rolling end point (at the end of l_R) of the strips. Figure S8 shows that strips have either a symmetric buckling mode shape (cleavage) as in θ = [20,35,45] or both buckle in the same direction as in θ = [25,35,40].

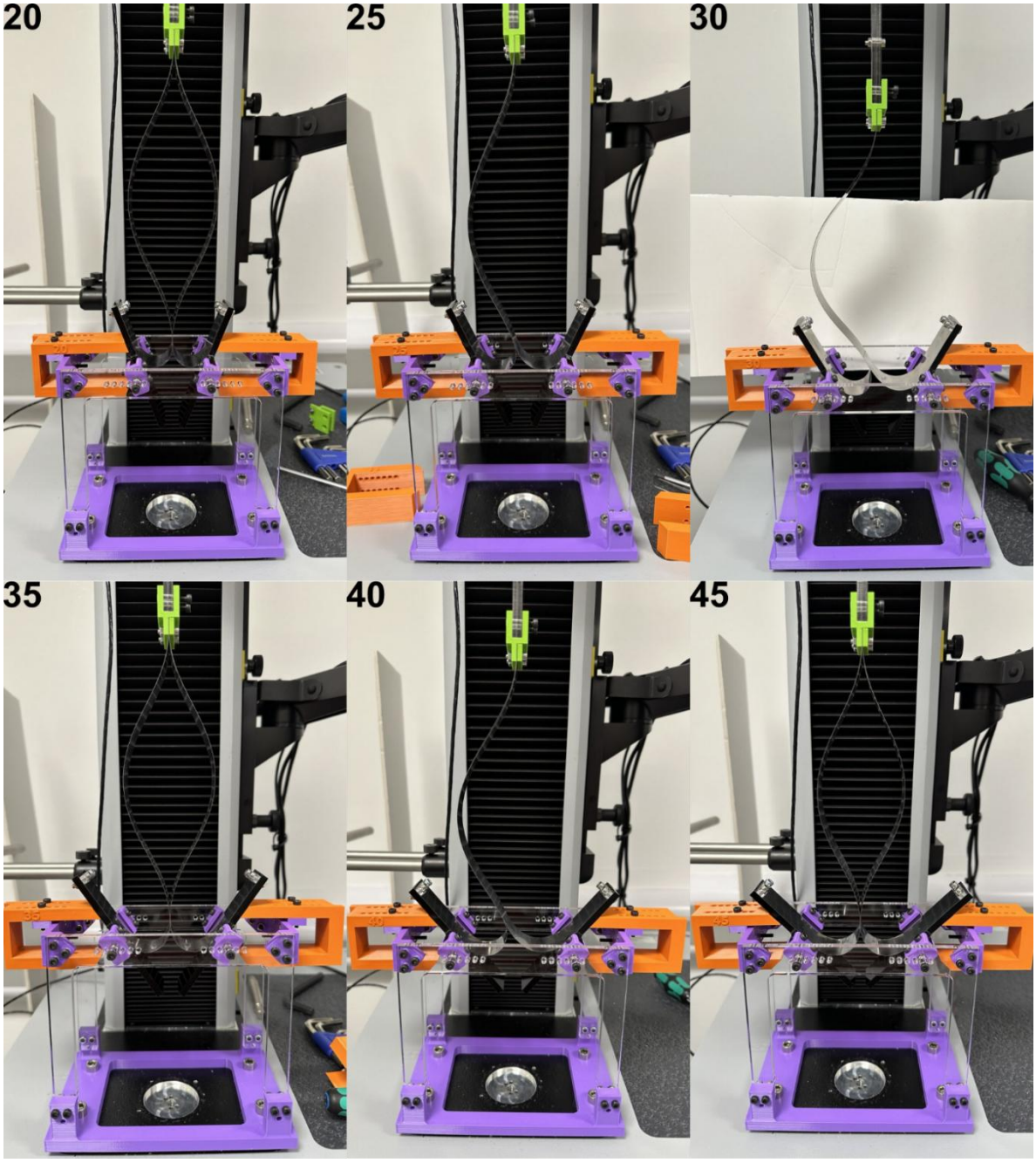

Figure S 8. The buckling mode shapes of strips in a test setup with W = 70 mm, t = 200 um, and different angles.

To understand the effect of boundary conditions, Equation S26 presents the relationship between the critical buckling load, modulus of elasticity E, moment of area I, length of the rolling section l_R, and the effective length factor, K, that depends on the boundary conditions at both ends.

$$P_{cr} = \frac{\pi^2 EI}{(Kl_R)^2} \qquad \text{S26}$$

Since one end of the strips is clamped, the boundary condition of the rolling end point is important. If the rolling end point is perfectly pinned, $K = 0.699$ and if it is clamped, $K = 0.5$. To understand better, we used numerical simulation where rolling length l_R, force and buckling

threshold could be measured. For three cases with angles θ = [30,40,45], t = 100 um, W = 60 mm, and l_S = 250 mm, we performed FE analysis using Abaqus as described in section SI.3. The results are presented in Table S3.

Table S 3. Buckling load values from FE analysis in comparison to analytical values for critical buckling load for pinned-clamp and clamp-clamp boundary conditions.

	FE analysis		Analytical	
Angle θ	l_R (mm)	Force (N)	K = 0.699	K = 0.5
35	170	0.556	0.598	0.305
40	170	0.535	0.598	0.305
45	170	0.536	0.598	0.305

The results in Table S3 show that the buckling load values of the rolling case are lower than that of clamp-clamp but much more than that of pinned-clamp boundary condition. Therefore, it is concluded that the contact condition in the rolling strips case is not perfectly clamped but is more constrained than a pinned condition, which means that cannot freely rotate at the rolling end point. Hence, finding analytical solution for buckling analysis requires proper analysis of the boundary conditions elasticity at the rolling end [1,2]. The buckling mode shapes of the three cases with θ = [30,40,45] are shown in Figure S9, where clamped end is at the top.

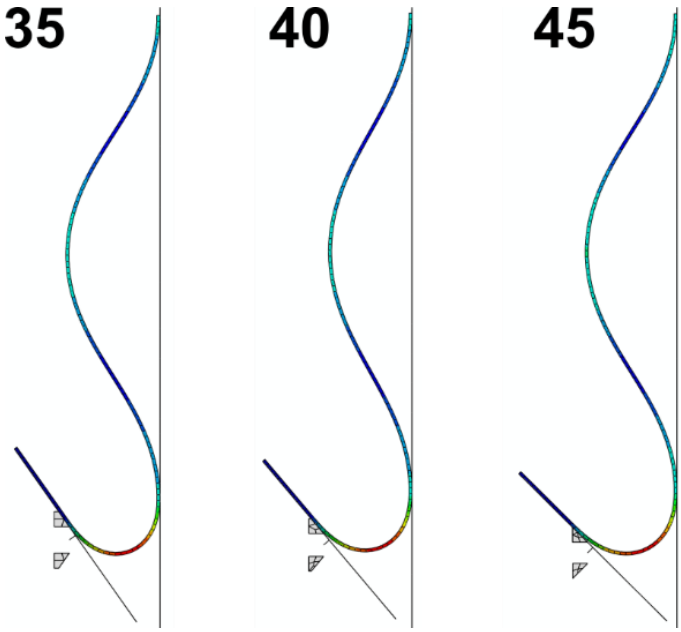

Figure S 9. Buckling modes of three cases with θ = [30,40,45] using FE analysis.

SI-1.8. Effect of material properties on performance

To evaluate the effect of the material on the performance of the bistable mechanism, further tensile tests experiments using mylar and PETG strips are performed, and the results are compared to those of a steel strip (Figure S11). The thicknesses of the strips are 250 microns (PETG) and 300 microns (mylar), and the width and length are as for the metal strips. The elastic modulus of the PETG and mylar are obtained by linear fitting the stress-strain data up to 0.01strain as shown in Figure S10. The PETG has a modulus E = 1612.2 ± 7.3 MPa, while mylar features a modulus value E = 2545.9 ± 68.4 MPa.

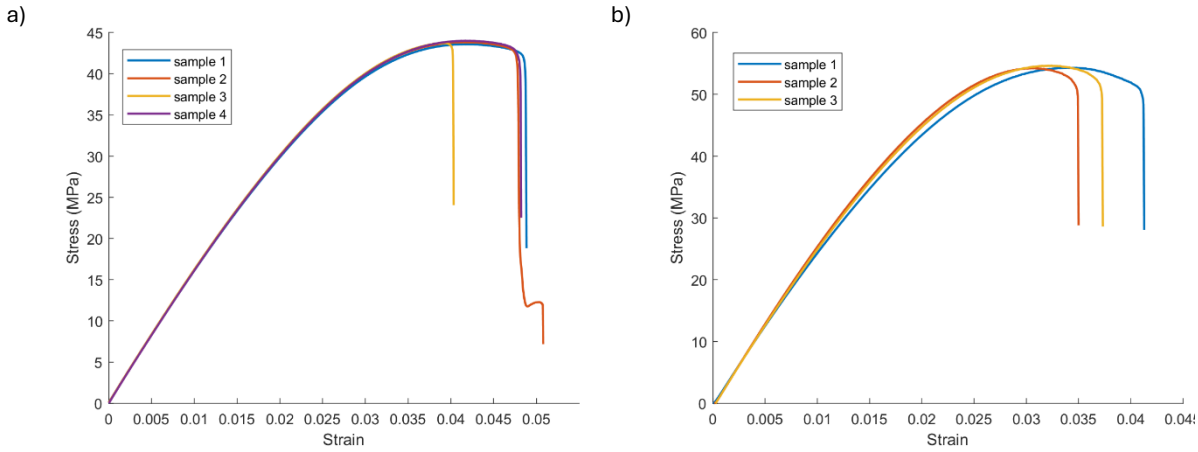

Figure S 10. Stress-strain diagrams of the tensile test specimens from a) PETG, and b) mylar.

Figure S11a shows the force-displacement diagrams of the steel (t = 200 microns), mylar and PETG strips, for θ = 20 degrees and W = 70 mm. The stiffness of the PETG and mylar strips are significantly lower than steel, therefore their stored strain energy and maximum force are significantly smaller than the steel case. For this reason, force-displacement data of the mylar and PETG strips are shown separately in Figure S11b for clarity. The measured forces are within the lower end of the load cell resolution; hence, imperfections affect the results and cause slight fluctuations in the mechanical response. It is however clear that force-displacement characteristics follow similar trends in terms of positive/negative stiffness and positive/negative force, noting that the values depend on the specific material considered.

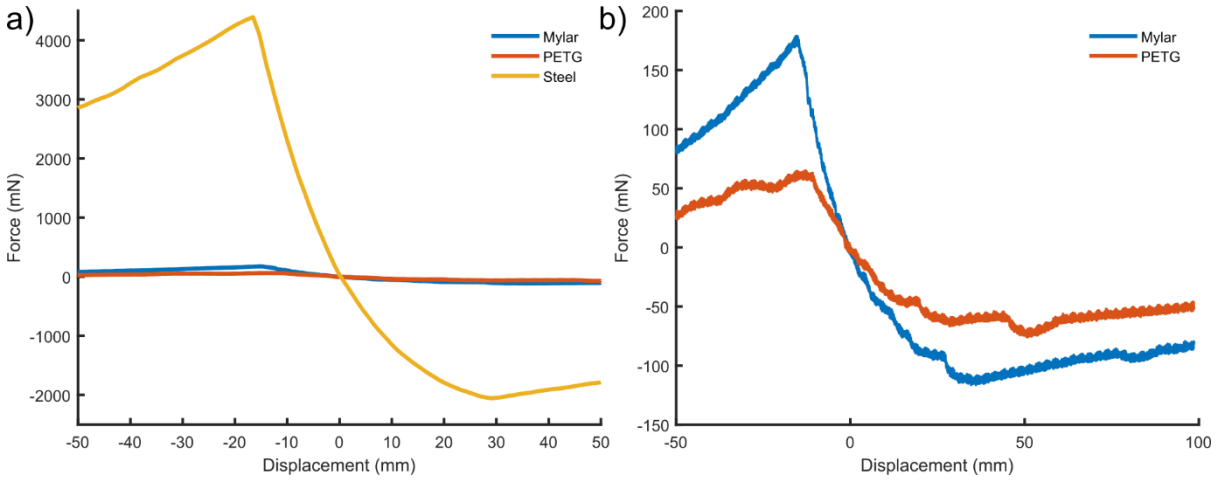

Figure S 11. (a) Force-displacement diagrams of the bistable mechanism with θ = 20 degrees and W = 70 mm for strips made of steel, mylar, and PETG, and (b) mylar and PETG only.

The maximum forces experienced by the strips were 65 mN, 179 mN and 4392 mN for PETG, mylar and steel, respectively. The characterization presented in Figure 2 of the manuscript shows effects from different geometrical parameters of the steel strips. To correlate data between steel and other materials, it is important to note that the axial force is a function of the strain energy, the latter being a function of the bending rigidity (EI). While the moment of inertia I is a function of strip geometry, the Young's modulus E incorporates the effect of the material. This is further shown in Table S4, where the ratios between maximum forces of PETG and mylar with respect to steel are compared to the ratio of their bending rigidities. One can observe a very close proximity of the two ratios. The maximum force could therefore be obtained from the ratio values provided for steel under different geometrical settings, as presented in the characterization diagrams of Figure 2 of the manuscript.

Table S 4. Comparison between the ratio of maximum forces in force-displacement diagrams of different materials versus the ratio of bending rigidity (EI).

Parameter	Maximum force ratio	Bending rigidity (*EI*) ratio
PETG/Steel	0.01478	0.01499
Mylar/Steel	0.04076	0.04092

SI-2. Mechanical test details

The mechanical test setup for the quasi-static characterization of the bistable mechanism is shown in Figure S12. The position of the hinges can change as a row of holes with 5 mm distance exist, allowing for tuning the width W. The angles on both convergent and divergent sides were equal and replaceable angle stoppers for every 5 degrees angle within the range θ = [5,45] were 3D-printed and used for each test. Each test was performed with 100 mm/min speed, and two compression-tension cycles were recorded as shown in supplementary video (SV-1).

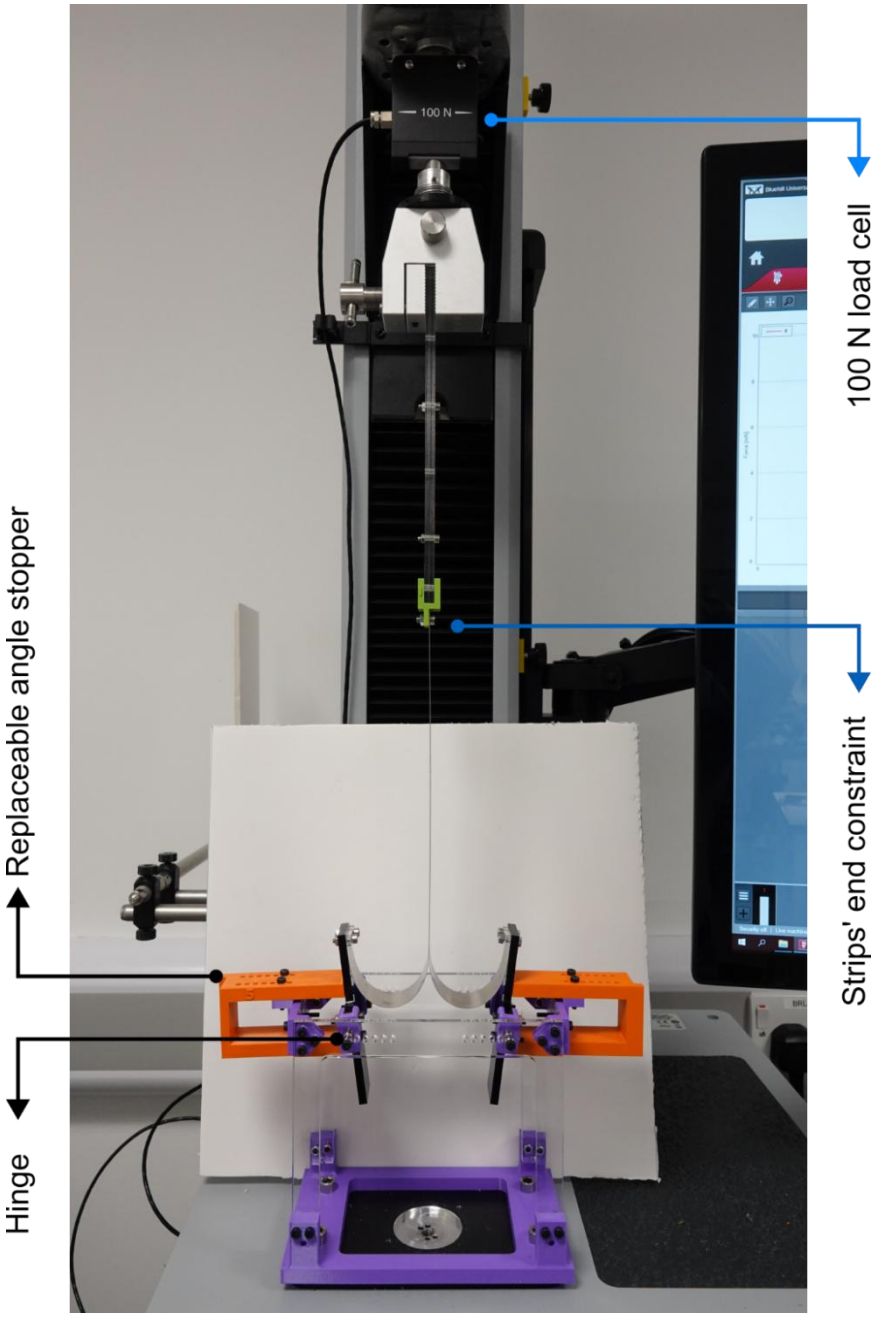

Figure S 12- Tensile test setup for bistable mechanism characterization

The combined plot of force-displacement diagrams for t =100, 150, 200 um are presented in Figures S13-S15, respectively.

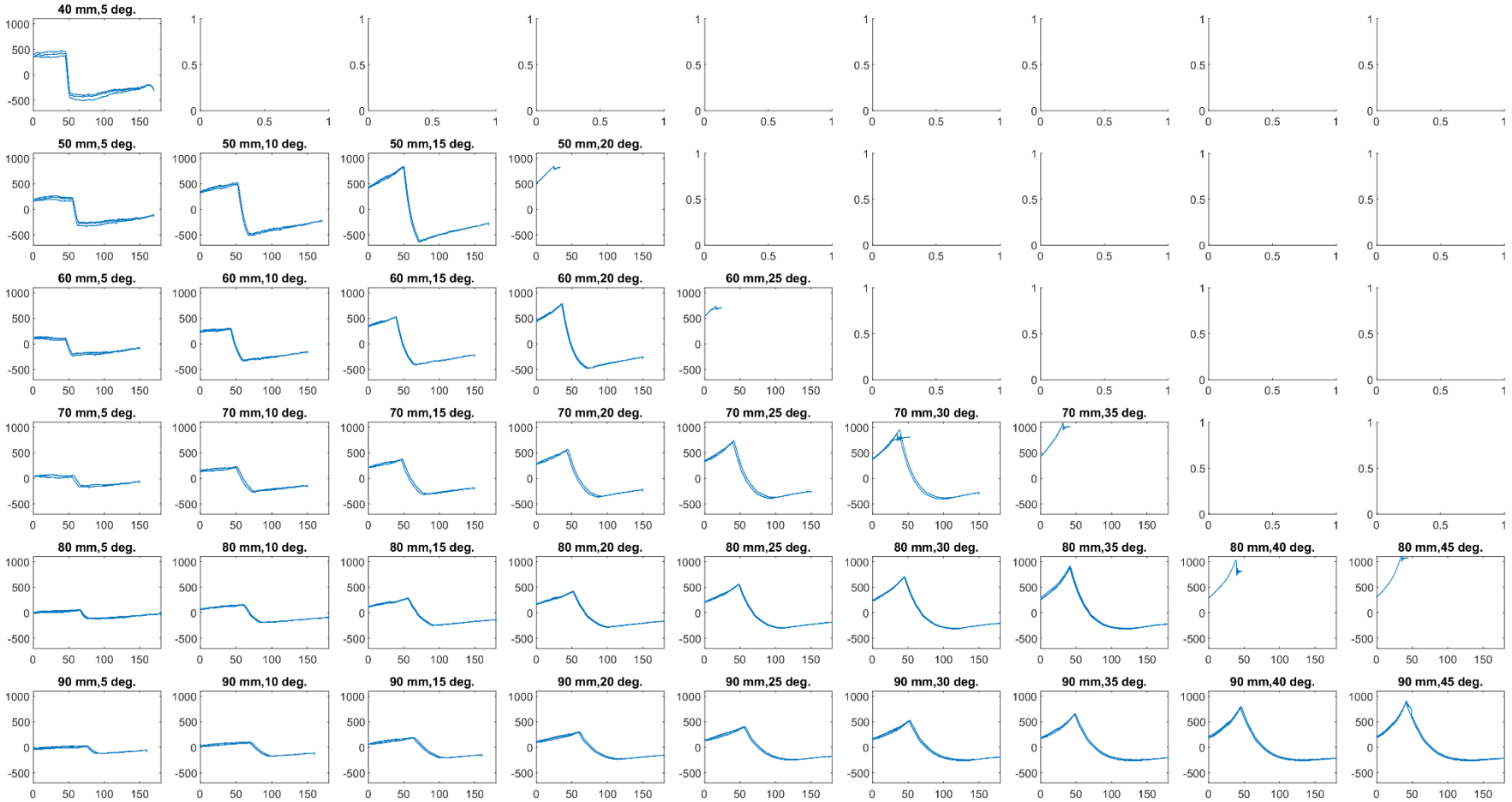

Figure S 13- Combined force-displacement diagrams of t = 100 um.

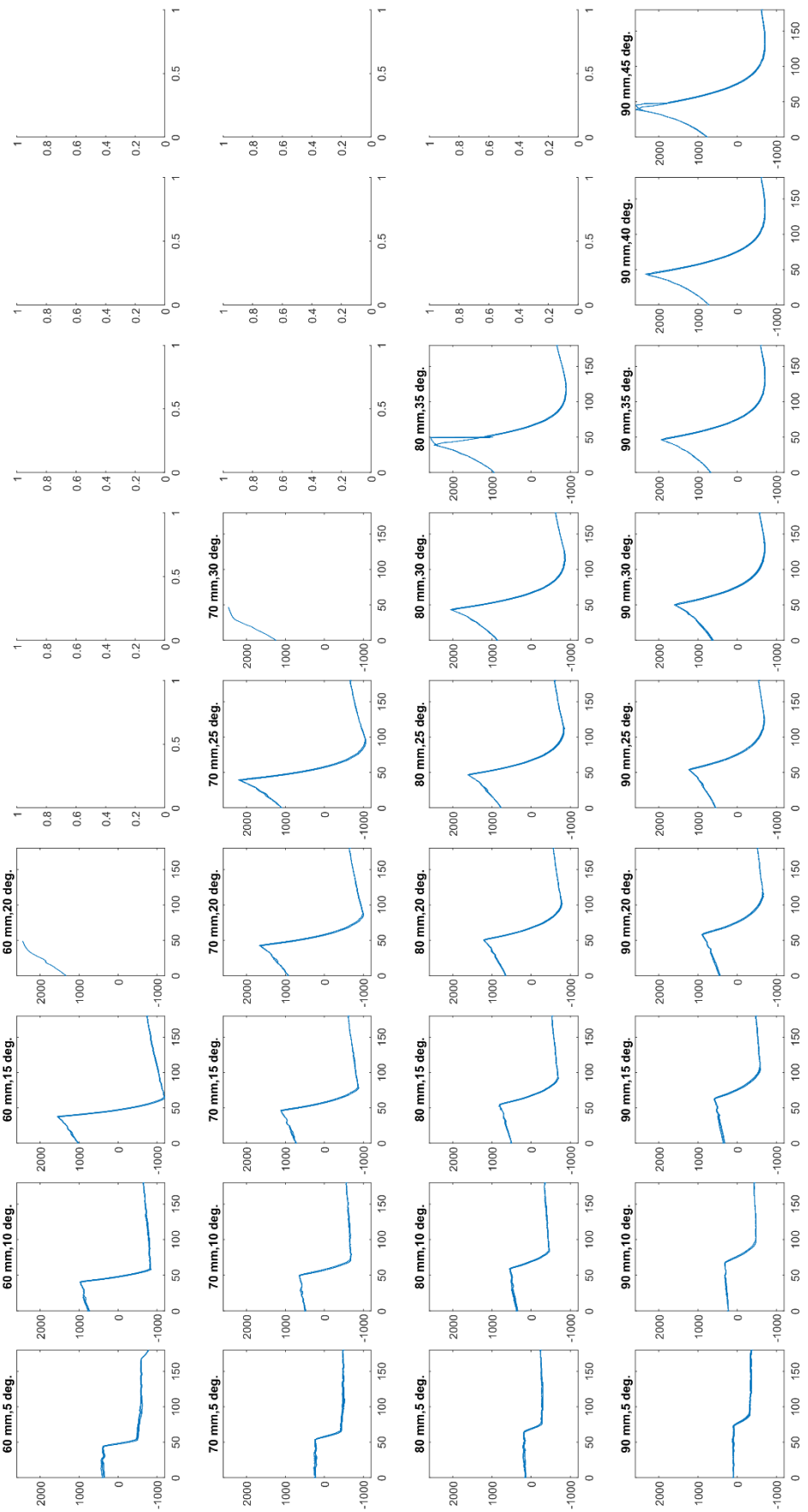

Figure S 14- Combined force-displacement diagrams of t = 150 um.

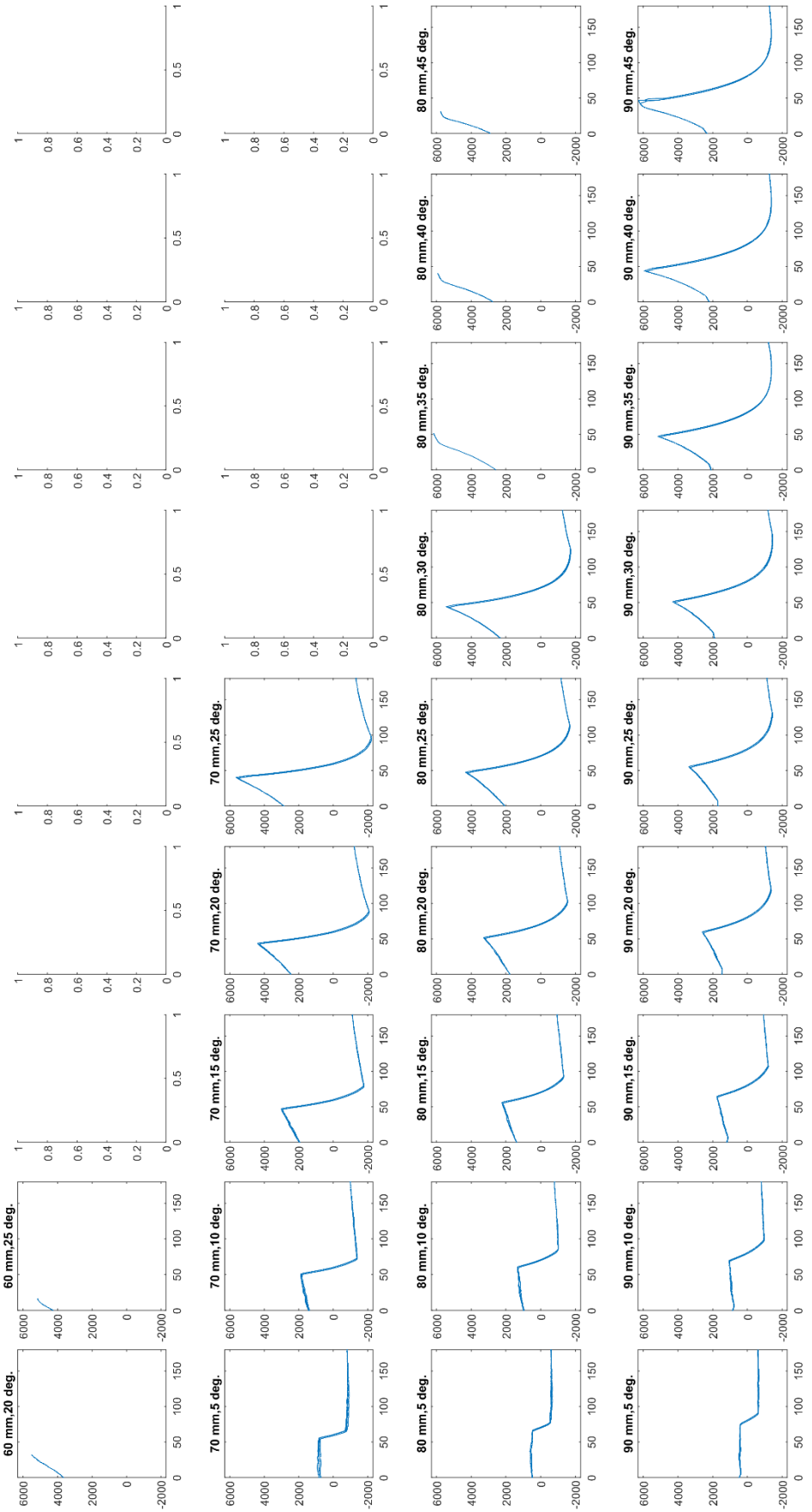

Figure S 15- Combined force-displacement diagrams of t = 200 um.

SI-3. Finite element analysis details.

Finite element analysis was performed using Abaqus 2023. The model was created by considering the rotating wall and angle stoppers (Figure S16a & S16b) as discrete rigid components and the metal strip was an elastic body. To improve the simulation efficiency, the model was simplified by considering a symmetry condition, i.e., half the mechanism was created for solution, hence, a symmetry wall was introduced at the distance $W/2$ from the hinge position.

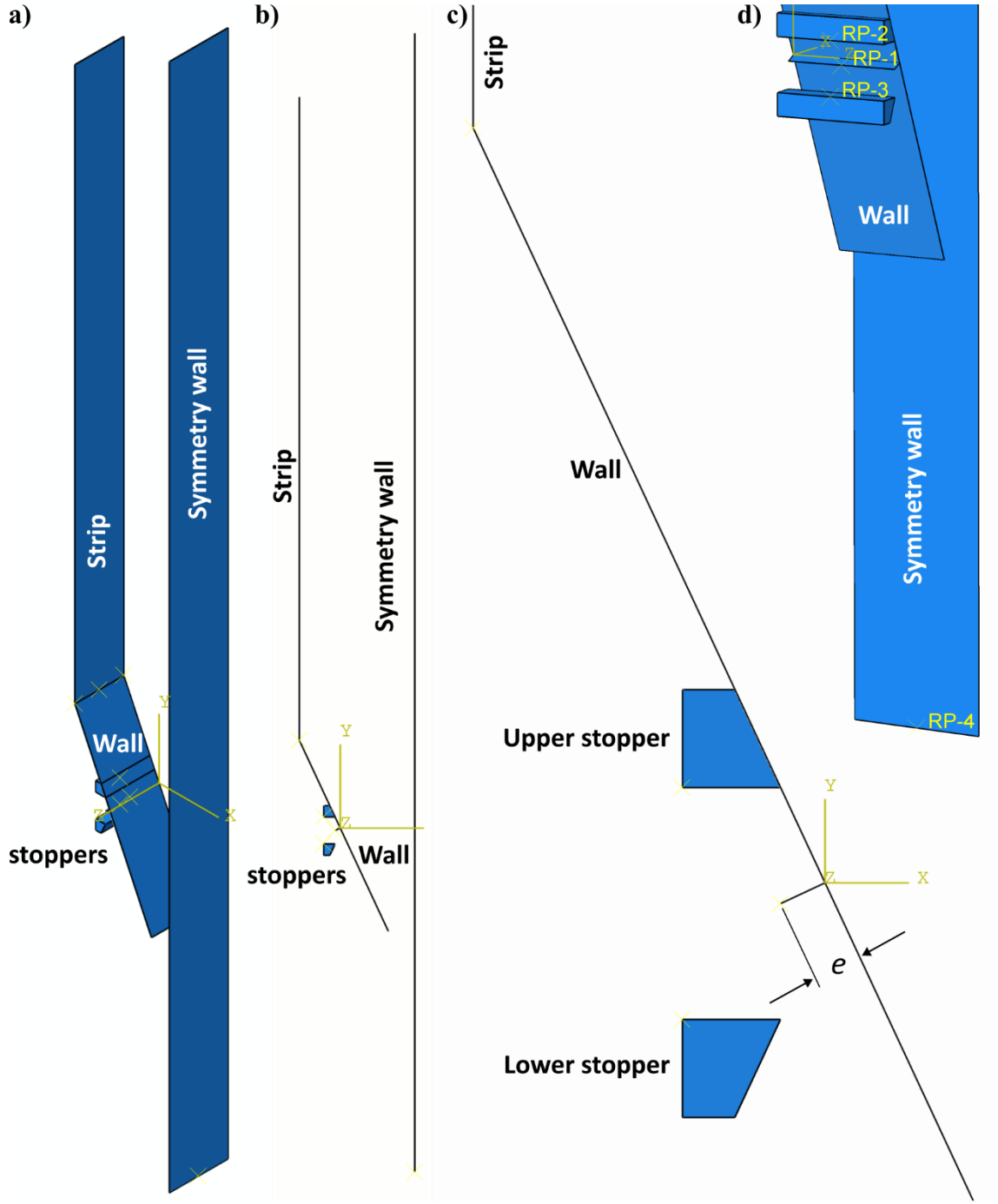

Figure S 16- The assembled model for the finite element analysis in Abaqus 2023 environment. a) isometric view of the model, b) front view, c) zoomed section of the front view, and d) definition of the reference points.

To replicate the contact between two strips, the symmetry wall was modelled as discrete rigid wall without friction. The friction was neglected because the two strips in back-to-back contact roll together and do not slide with respect to each other. The rotating wall was created as a rigid shell where the thickness of the wall (and eccentricity) was addressed with a rib with length equal to e ($e = T/2$), as shown in Figure S16c. The rotating wall, stoppers, and symmetry wall were rigidly coupled to reference points RP-1 to RP-4, respectively (Figure S16d). The position of the stoppers was constant through the simulations as they will be later used to measure the transvers forces (in x-direction within the coordinate system shown in Figure S16c).

The material properties used were linear elastic with modulus E = 210 GPa (according to the supplier datasheet), density ρ = 7800 kg/m^3 and Poisson's ratio ν = 0.3. The assembly of the model parts are shown in Figure S16b. The selection of solver was limited due to the complexity and large area of contact in this model and nonlinear deformations in the strip, therefore, dynamic explicit method was used to capture the contact complexities. The solution consists of two dynamic explicit steps: 1) applying the initial deformation in the straight undeformed strip and 2) pushing the strip into the channel. In both steps, geometrical nonlinearity was considered in the solution. The solution time and implementation of the quasi-static condition is governed by both the scale factor and step time. Therefore, the step time at step 1 was considered 100 s where scaling factor of 10,000 was applied to accelerate the computation time. The loading amplitude in this step was a smooth step with amp = 0 at t = 0 s and amp = 1 at t = 100 s. In second step, the loading speed was reduced by choosing step time t = 200 s and reducing the scaling factor to 100. To stabilize the solution further and reduce the noise due to the wave propagation in the strip, damping ratio β = 5E-07, which is smaller than the increment size was also introduced in material properties. In order to reduce the kinetic energy inherited from step 1, the loading amplitude of smooth step was considered with 5 s of no loading at the beginning, which means amp = 0 at t = 0 s (step time), amp = 0 at t = 5 s, and amp = 1 at t = 200 s.

To replicate the quasi-static and displacement-controlled condition of the experimental tensile tests, displacement-controlled boundary conditions were applied. The set of boundary conditions applied in general is shown in Figure S17a for both steps where only rotational degree UR3 was allowed at the hinge (RP-1) as shown in Figure S17b. The boundary condition at reference points RP-2, RP-3, and RP-4 was Encastre through the whole simulation steps. The strip has two ends: one at the top (as shown in Figure S16a) and one at the bottom that constrains the rotating wall. The set of boundary conditions at the bottom of the strip that do not change through simulation steps are constrained initially as shown in Figure S17c. In step 1, the displacements on the strip's bottom (Figure S17d) are constrained while the rotation equal to ($180 - \theta$) is applied (θ=25° in this case in Radians). In step 2, the rotations and displacements, apart from those initially constrained, are allowed free (Figure S17e) because the nodes at the bottom of the strip are coupled to a reference point at the top of the rotating wall using a pin constraint.

The set of boundary conditions at the top of the strip that do not change through simulation steps are constrained initially as shown in Figure S17f. The displacements U1 and U2 defined in this step bring the top position of the strip to the contact point with symmetry wall at the distance L from the hinge. In step 2, the displacement of 180 mm, similar to the experimental

tests, is applied at the top of the strip where the sum of reaction forces at the top of strip were measured to derive force-displacement profile at every one second point (200 points).

The history output and field output at step 2 were requested every second and the amount of kinetic energy compared to the internal energy was monitored where the ratio of kinetic to internal energy was maintained below 10^{-4} through the simulation in both steps. In terms of contact, general contact at initial step was defined with frictionless tangential and hard contact normal behaviors. The contact between the strip and the rotating wall followed a surface-to-surface contact with penalty method. The strip was then discretized using explicit S4R elements with approximate global size of 2 mm.

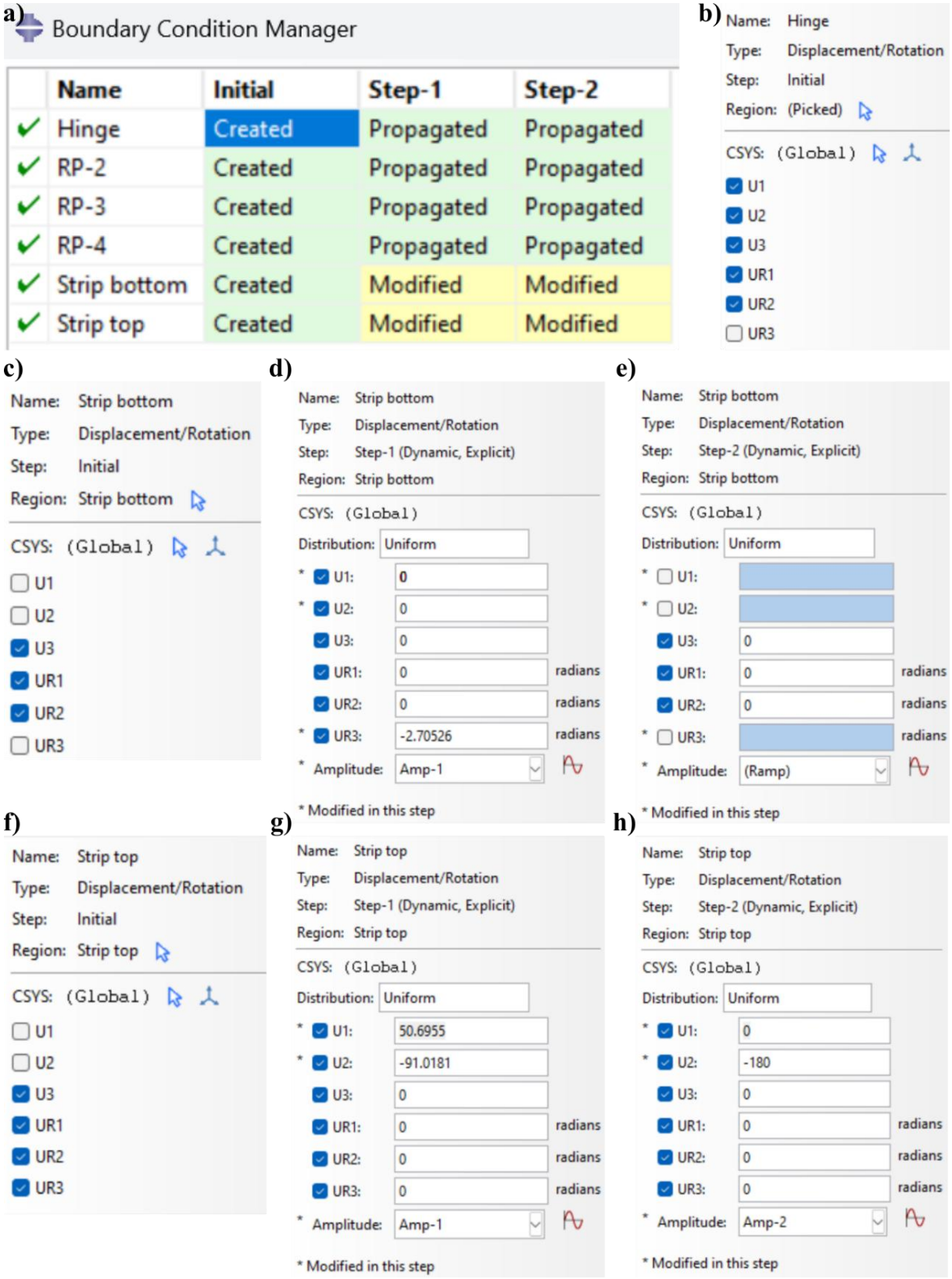

Figure S 17- Definition of the boundary conditions at different positions of the model for different steps.

SI-4. Lattice test details.

The test setup for the lattice and the frame to impose the boundary conditions are presented below.

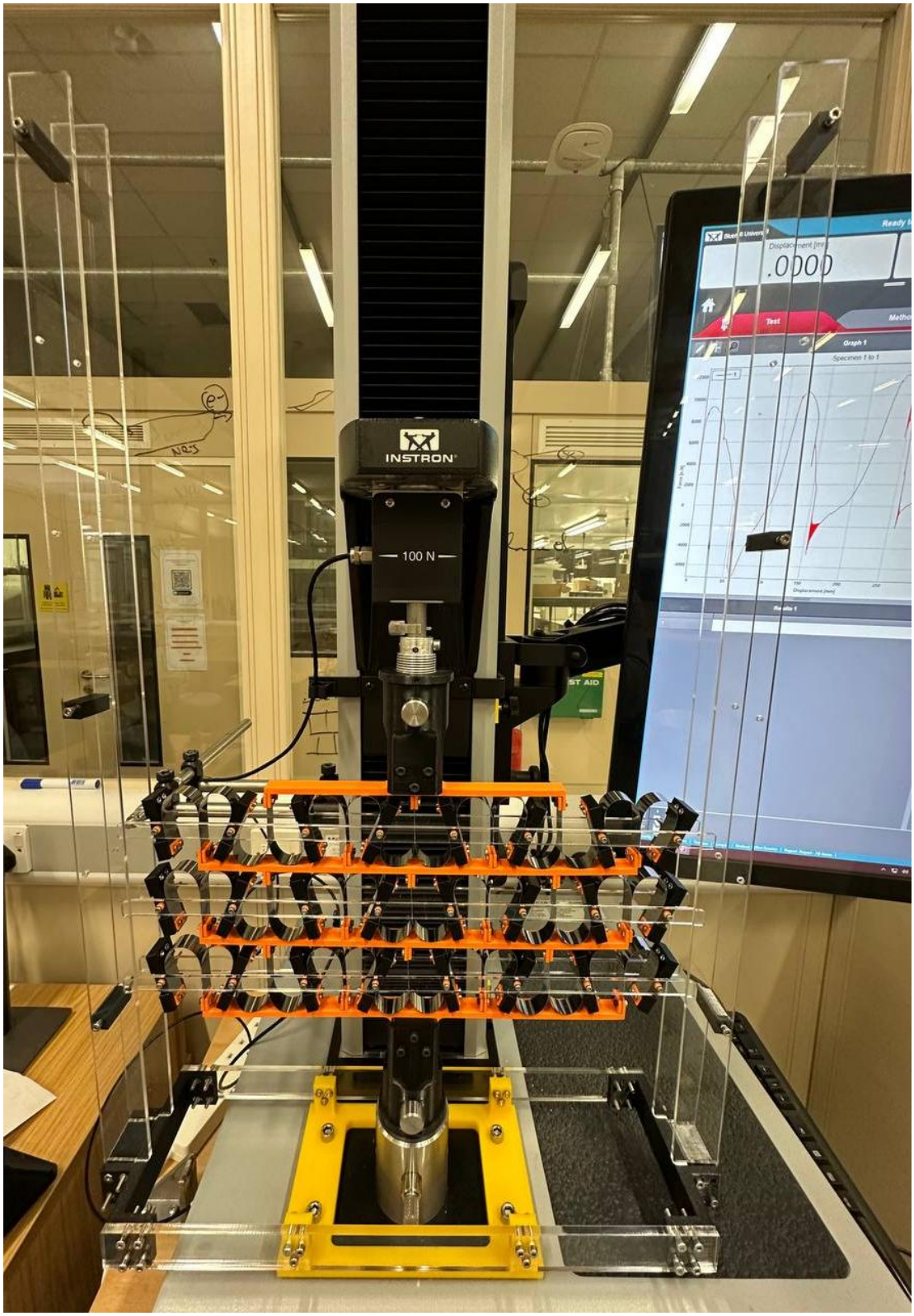

Figure S 18- Lattice tensile test setup including the frame supporting the edges against out-of-plane deformation and buckling.

SI-5. Multi strip design details.

The multistrip design imposes some complexities in terms of design calculations. Here, we make some assumptions to simplify the problem. First, we assume that the width W is much larger than thickness of the strips t. Therefore, the difference in force-displacement profile of different strips in a layered stack is negligible. In addition, we assume that the force-displacement profile of the individual strips in the positive stiffness range is approximately linear although nonlinear profiles are also easy to calculate once the nonlinear relation is known.

Consider three strips 1, 2, and 3 as shown in Figure S19a, which exert contact forces f_1, f_2, and f_3 on the rotating wall surface, respectively. If length difference between the strips is Δl_S, then the difference in the wall contact length of the strips $\Delta l_W = \Delta l_S / 2$ and similarly for Δl_R. The contact forces exerted by each strip is different to curvature difference. In order to understand the displacement at which maximum force occurs (onset of wall rotation), it is easier to evaluate the equivalent contact force. The equivalent force (resultant force) is much larger than every single strip's contact force and its position could be estimated by finding the centroid of these single contact forces.

For a specific case discussed in the manuscript and shown here in Figure S19b, the length difference of strips is Δl_S = 10 mm. We call the distance of the maximum force of the multi-strip case from that of a single strip, d_{cent}, which addresses the centroid distance. In addition, the total distance of the maximum load between single strips is $d_{tot} = (n-1) \times \Delta l_S$ (if length difference between strips is constant). Assuming a linear force-displacement response at positive stiffness range for each strip, the centroid distance will be the resultant of the centroid of a right angle triangle as $d_{cent}^{tri} = d_{tot}/3$ and a rectangle as $d_{cent}^{rec} = d_{tot}/2$ as shown in Figure S19c. The resultant centroid could be obtained from Equation S27.

$$d_{cent} = \frac{d_{cent}^{rec} \times A_{rec} + d_{cent}^{tri} \times A_{tri}}{A_{rec} + A_{tri}} \qquad \text{S27}$$

where A_{rec} and A_{tri} are the area of the rectangular and triangular parts, respectively. The value of the minimum force, f_{min}, in Figure S19c is the force of the 5th strip (red) at the displacement where maximum force for the 1st strip (blue) occurs. Considering the case shown in Figure S19b, the centroidal distance from Equation S27 was 17.46 mm and from experimental results was 16.49 mm, which means about 6.5% relative error. Therefore, this method proves to be a proper approximation for the maximum force distance in a multi-strip case.

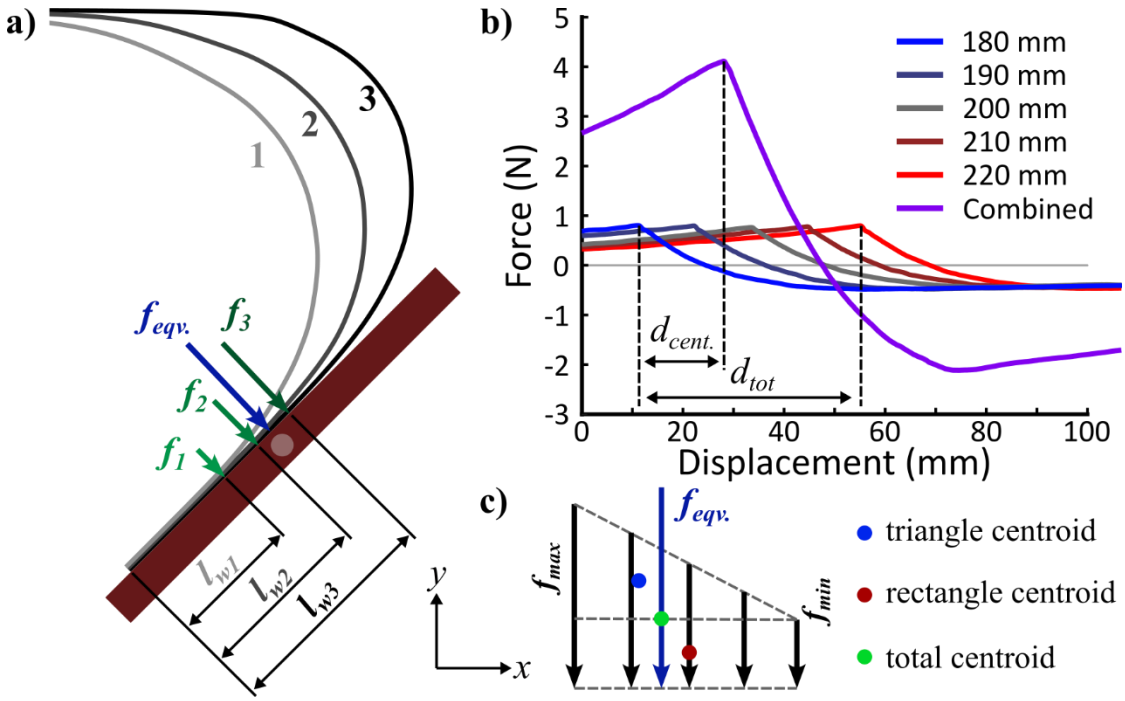

Figure S 19. ***Multi-strip design.*** *Transition load position in multi-strip design, a) illustration of contact point loads of each strip with respect to rotating hinge, b) an example of maximum load position for individual and combined strips (length of different strips are given in the legend), and c) centroidal equivalent force definition.*

SI-6. Actuation study details.

The cumulative displacement diagrams of actuation for 5 g and 10 g masses for both angle and width studies are presented in Figure S20.

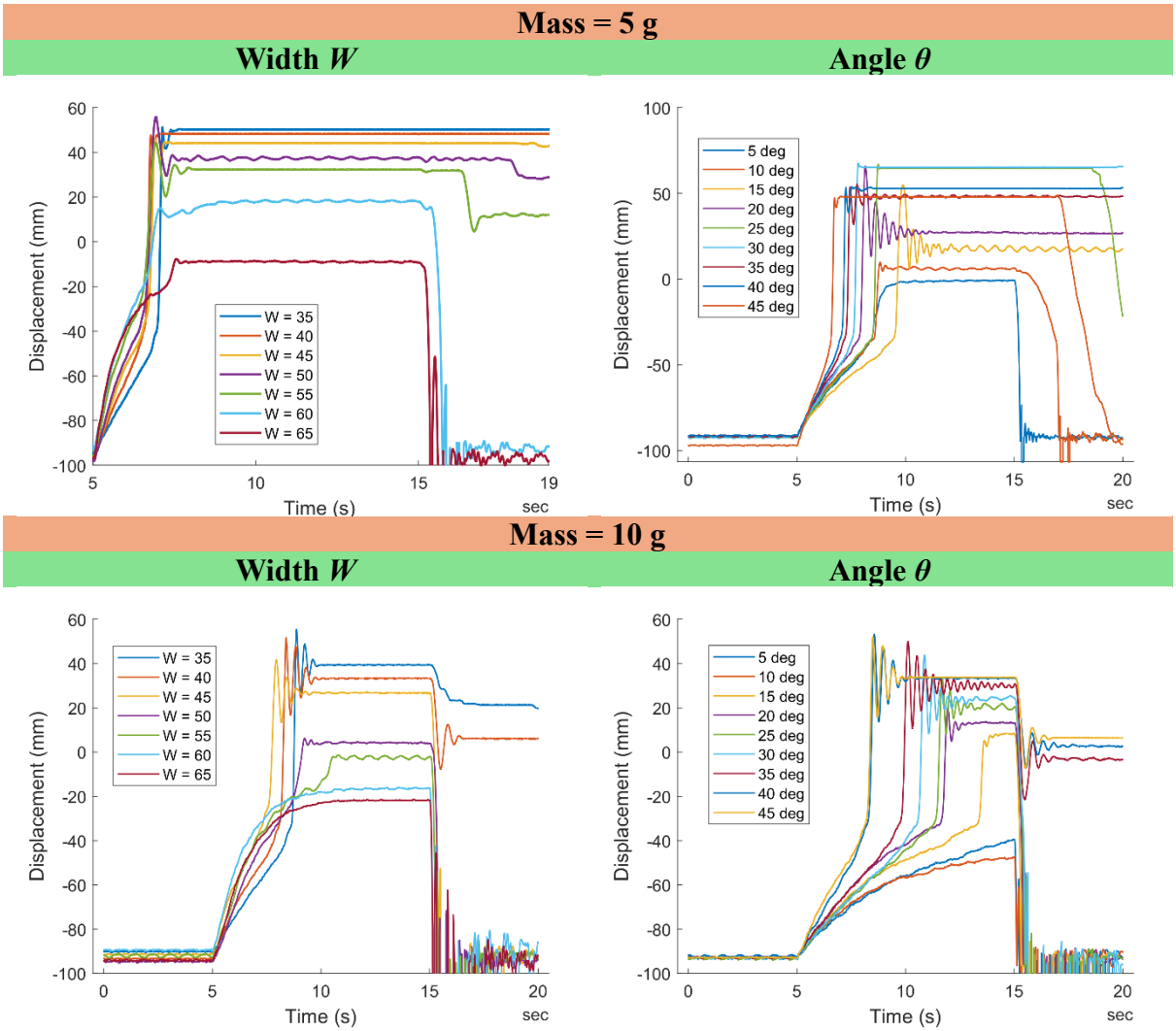

Figure S 20- Cumulative actuation diagrams for two hanging masses of 5g and 10g in isotonic characterization study.

The electrostatic zipping actuators have a capacitance and using a parallel plate capacitor model, this capacitance can be calculated [3-5]. The capacitance can be calculated using Equation S28.

$$C = \frac{\varepsilon_r \varepsilon_0 A}{T} \qquad \text{S28}$$

where ε_0 and ε_r are the permittivity of free space and the relative permittivity of the dielectric, respectively, and T is the thickness of the dielectric. Considering the geometrical parameters of the rolling mechanism shown in Figure S21c, area A could be calculated as

$$A = b.l_W \qquad \text{S29}$$

where b is the out-of-plane width of the wall and l_W is the length of strip that is in contact with the wall. The leakage current was found to be linearly correlated to the capacitance and could

be calculated by having the actuation voltage [3,4], hence it is possible to correlate the leakage current to l_W, since b is constant and area A depends on l_W only. This requires a proper measurement of the dielectric thickness and the relative permittivity values.

Figure S21d shows the leakage current versus the measured displacement using a laser sensor, which represents the rolling length l_R. The figure suggests that there exists a range (highlighted using green dashed line) with linear correlation between rolling displacement and current. As described in section SI-1, rolling length and wall contact length could be found using ellipse fitting method. Therefore, it could be possible to develop and calibrate a self-sensing model for a specific actuator in the future that maps the rolling displacement to the current. One important point is that once $l_W > l_c$, snapping and switching to the second state has occurred. Although developing and calibrating a sensing model to measure l_W is difficult, it is possible to calibrate a model to assess switching of stable states.

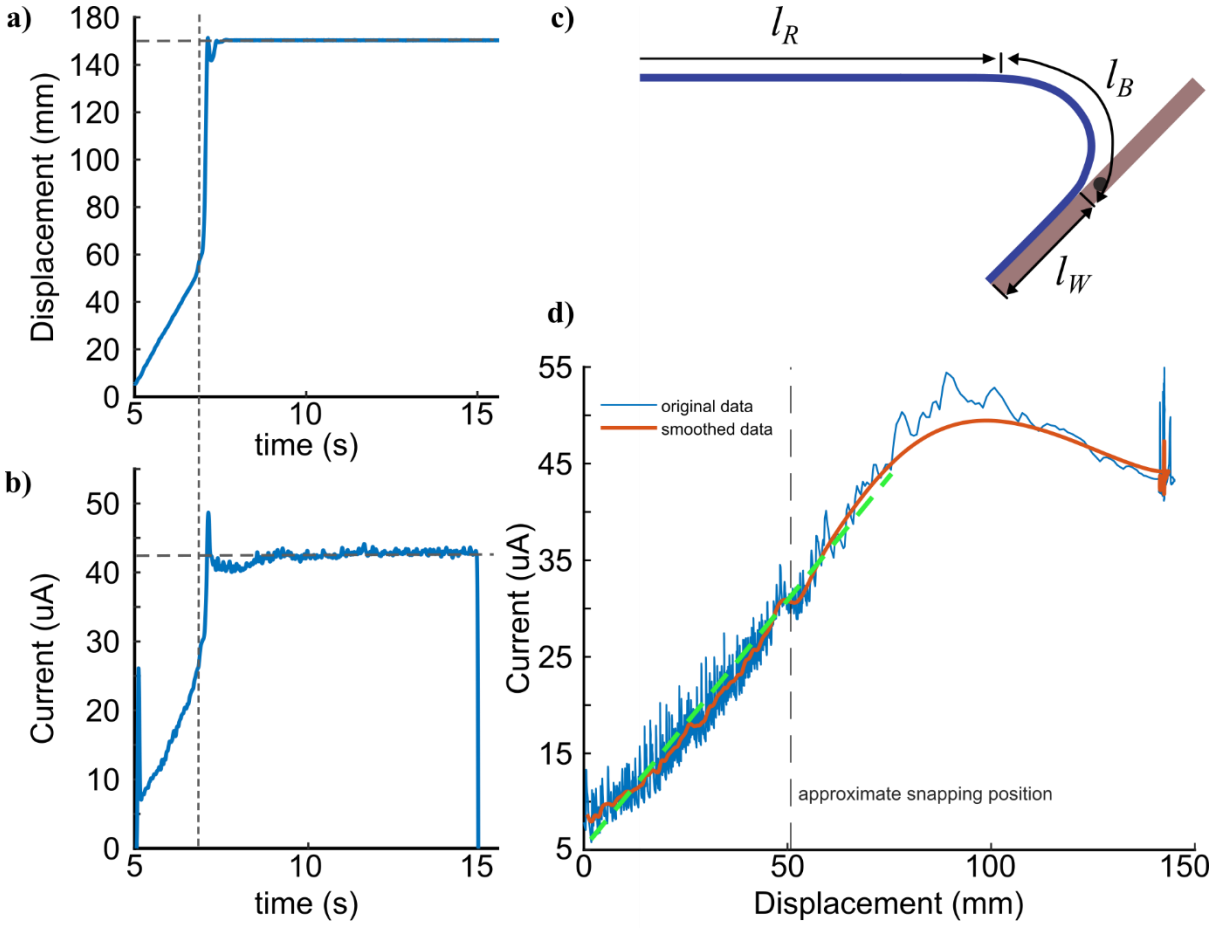

Figure S 21- Current sensing model. a) variation of displacement with actuation time, b) variation of parasitic current leakage with actuation time, c) definition of the contact length on the rotating wall l_w, and d) variation of current with displacement.

SI-7. Perching mechanism study details.

In contrast to the metamaterial design where angle stoppers are used, the perching mechanism has no angle stoppers but instead employs an axial displacement stopper for the strips as shown in Figure S22a. The position of the axial stopper ($d_{stopper}$) determines the actuation displacement (d_{act}) and the maximum actuation force (f_{act}) needed to activate the mechanism and pass through the snapping point (Figure S22b). As no angle stopper exists on the rotating wall, the length of the strip on the rotating wall (l_W) remains constant before snapping and the resultant contact force f is on the hinge as shown in Figure S22c. Once the mechanism passes the snapping point, the axial force becomes negative, however, the rotating walls immediately contact with the test target (PLA cylinder) that causes a jump in the force-displacement diagram.

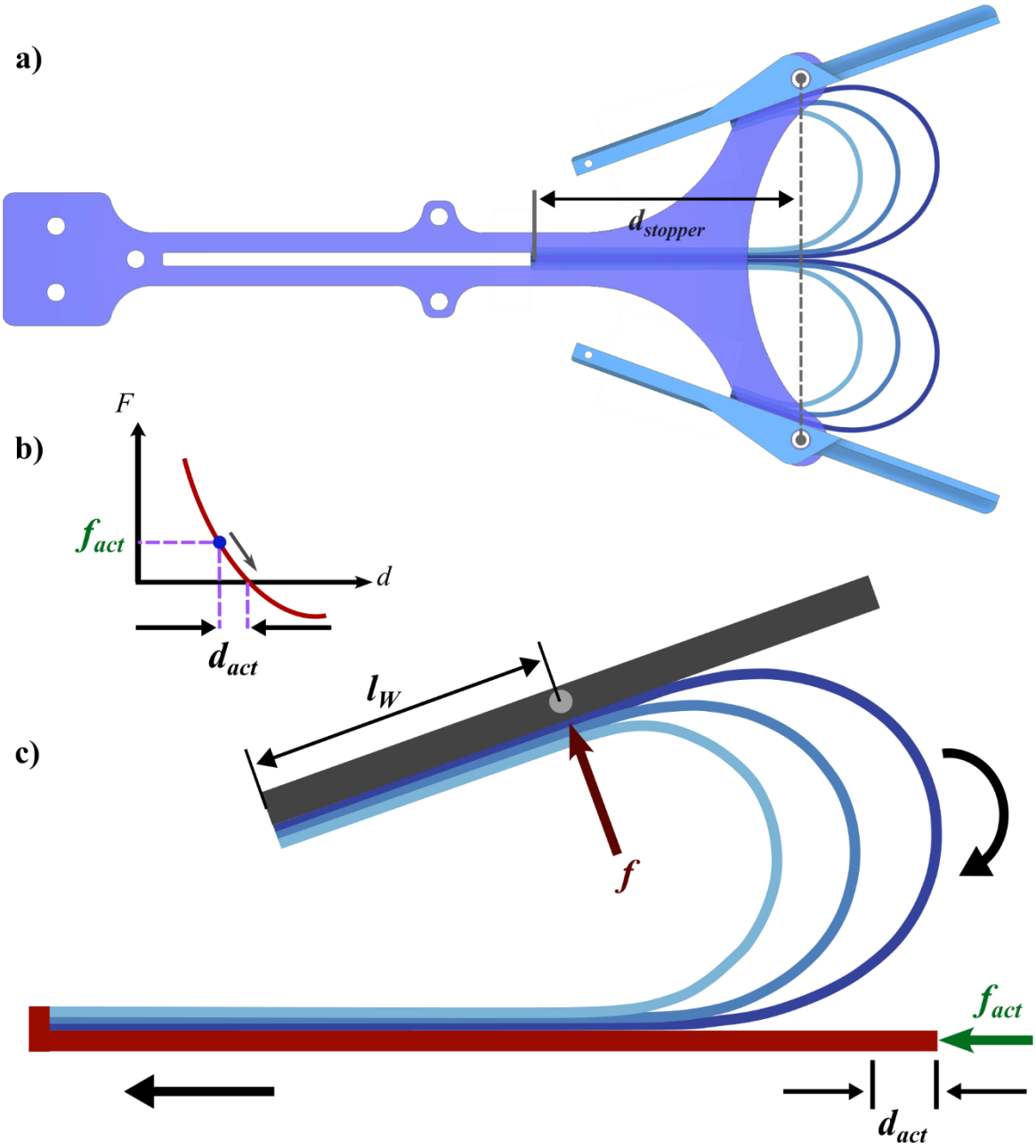

Figure S 22- Perching mechanism details and the definition of a) stopper distance, and b) activation distance.

To facilitate interpretation of the characterization diagrams in Figures 5f–5i, a representative force-displacement diagram for a cylinder with $D = 40$ mm cylinder is detailed in Figure S23. The contact initiation and snapping point are highlighted where the distance between these two is the activation displacement. The diagram shows that the maximum activation force is at the beginning of the contact (as described in Figure S22b), therefore, the smaller activation displacement results in smaller activation force. This is an advantage of the proposed perching mechanism with rolling strips where activation force and displacement can be tuned simply by tailoring the stopper distance ($d_{stopper}$).

The value of the force after snapping could be negative or positive. For the $D = 40$ mm cylinder shown here, the axial force post-snapping is close to zero, while for $D = 50$ mm cylinder it becomes positive and for cylinders smaller than $D = 40$ mm, it is negative (Figure 5f). The maximum downward force is achieved at the end of displacement range as highlighted in the figure, which depends on the number of strips and the target's diameter.

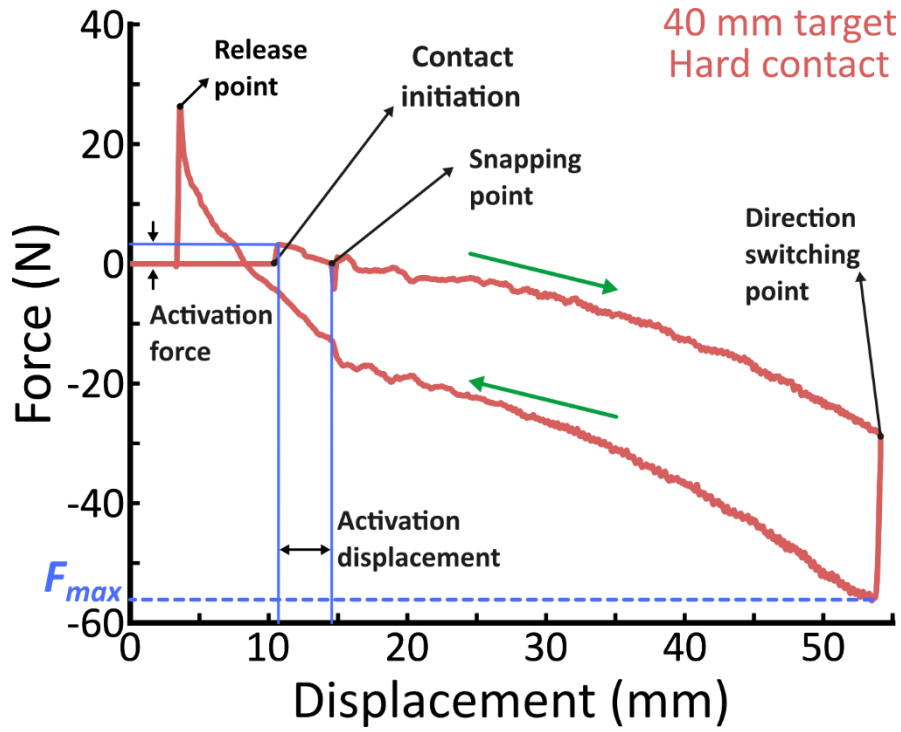

Figure S 23 - Interpretation of the force-displacement diagram of the perching mechanism during axial loading.

The test setup to measure the moment capacity is shown in Figure S24 where a removeable cylindrical target with different diameters is fastened to two drums. The drums are connected with steel threads to the linear motion head of the tensile test machine. The diameter of the thread spool is 40 mm; therefore, it is possible to convert the measured linear tensile force into the moment using formula $M = r.F$, where r is the radius equal to 40/2 = 20 mm and axial force F is measured by the load cell. In the test setup, the perching mechanism is clamped to the base where a sliding clamp is designed to allow linear adjustment of the perching foot position for different target diameters.

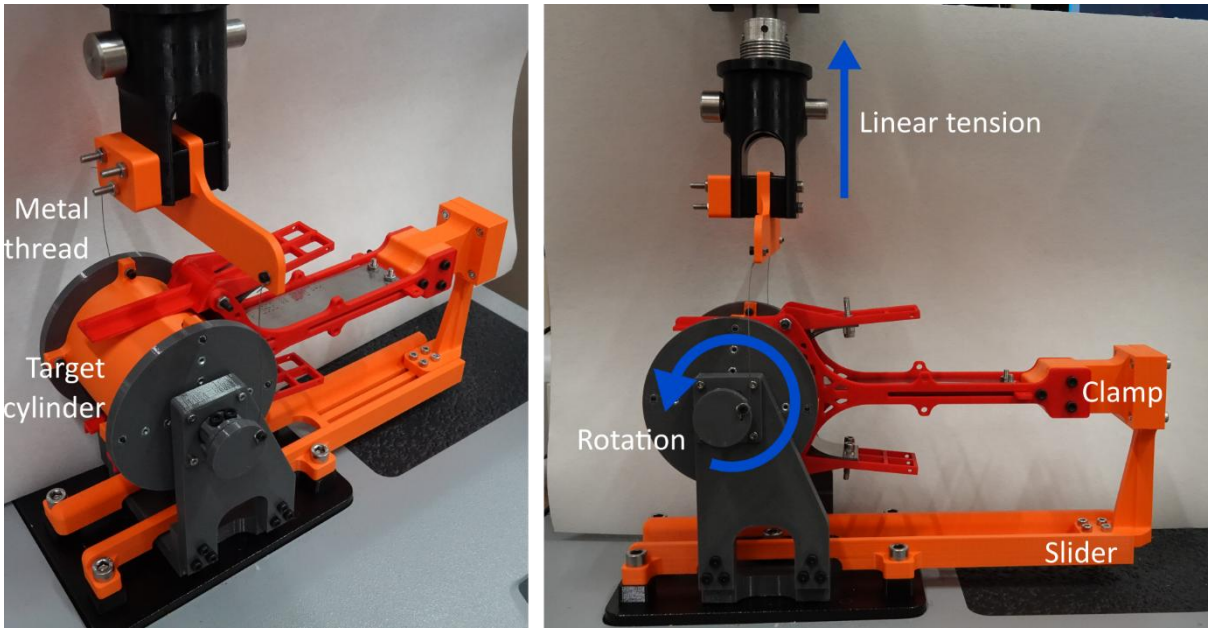

Figure S 24 - The mechanical test setup for measuring the moment capacity of the perching mechanism.

One important difference observed in the results is due to the contact surface properties of the walls and the target. Two cases of hard contact (flat PLA surface) and soft contact (silicone pad with Shore 30A) were studied. While contact surface properties affect the axial force-displacement profile, its impact on the moment capacity is much larger, where soft contact can provide more than double the moment capacity of the hard contact case. This difference mainly stems from the difference in contact area as illustrated in Figure S25. For the hard PLA surface, the contact surface between target and the wall is mainly a line, while for a silicone pad there is a large contact area due to the deformation of the silicone under normal contact stress. The silicone pad provides both larger coefficient of friction and larger contact area, hence the frictional shear stress significantly improves the moment capacity of the soft contact case. In addition, Supplementary Video 5 provides a better view of elastic deformations of the soft contact pad under axial loading tests.

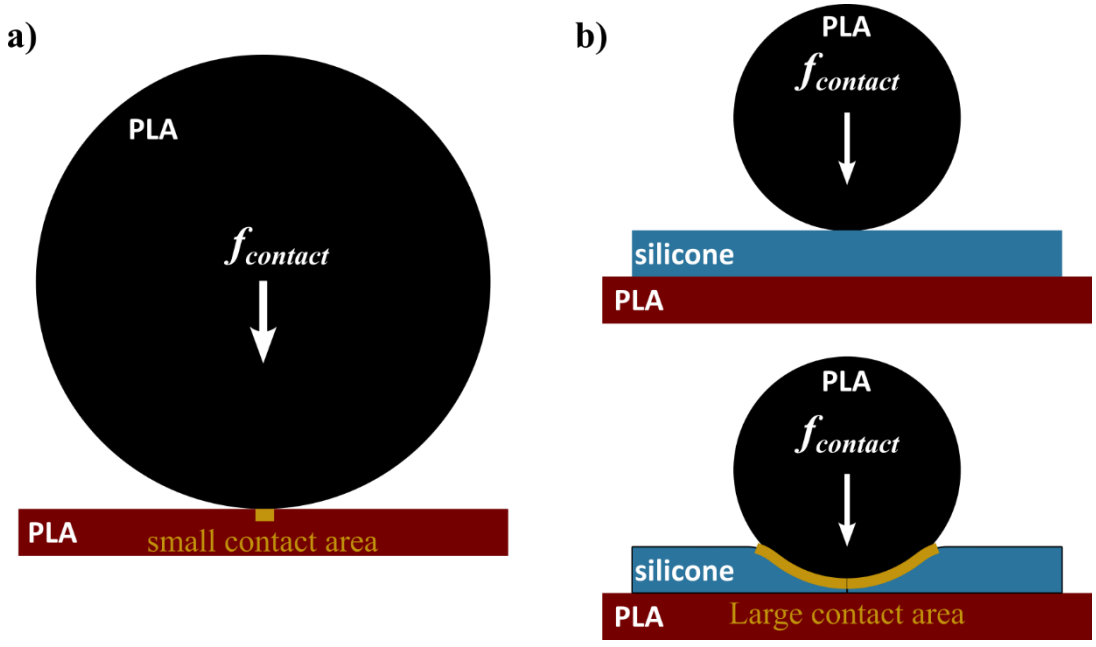

Figure S 25- Illustration of difference between: a) hard contact, and b) soft contact.

SI-8. Gripper design details.

The key aspect of the gripper design is leveraging the rotational motion of the walls. In order to have a deterministic range of motion and rotation angles, gripper design includes rotational angle stoppers as discussed in the manuscript. Therefore, initial and final configuration and angles of each bistable cell of a gripper are known. This helps to use the analytical methodology of section SI-1 to determine the position of the axial stoppers that affect the moment capacity of the gripper, especially in the final state. The moment generated by each cell in its final configuration (M_f) defines the total moment capacity of the gripper. The larger the moment (M_f), the heavier the object that gripper can lift. To develop a predictive model for the moment generated by each bistable cell, it is essential to analyze the static equilibrium of forces in the final configuration. Figure S26a illustrates the geometry of the strip at initial configuration where three different length sections of the strip are highlighted. The contact point of the strip where contact force, f, is exerted is on the right side of the rotating wall's hinge. Hence, it creates a clockwise moment M_i that maintains each cell of the gripper in initial configuration with stability.

Once rotation is applied and the strip transits to its second stable state and final configuration, the position of the contact force on the rotating wall changes (Figure S26b-c). The value of the contact force is dependent on l_W and it is maximum at the wall rotation threshold, where the contact point is on the hinge. However, at this condition the moment will become zero, since the moment arm d_f is zero. Therefore, a contact point not located on the hinge is needed, which could be defined by choosing a value for l_W. With this value determined and the angle θ known, we can estimate the ellipse shape of the bent strip section and locate the position of the ellipse apex along the bisector line. Accounting for the strip's thickness, this point defines the position of the linear stopper, with coordinates (x_s ,y_s) in (x,y) coordinate system.

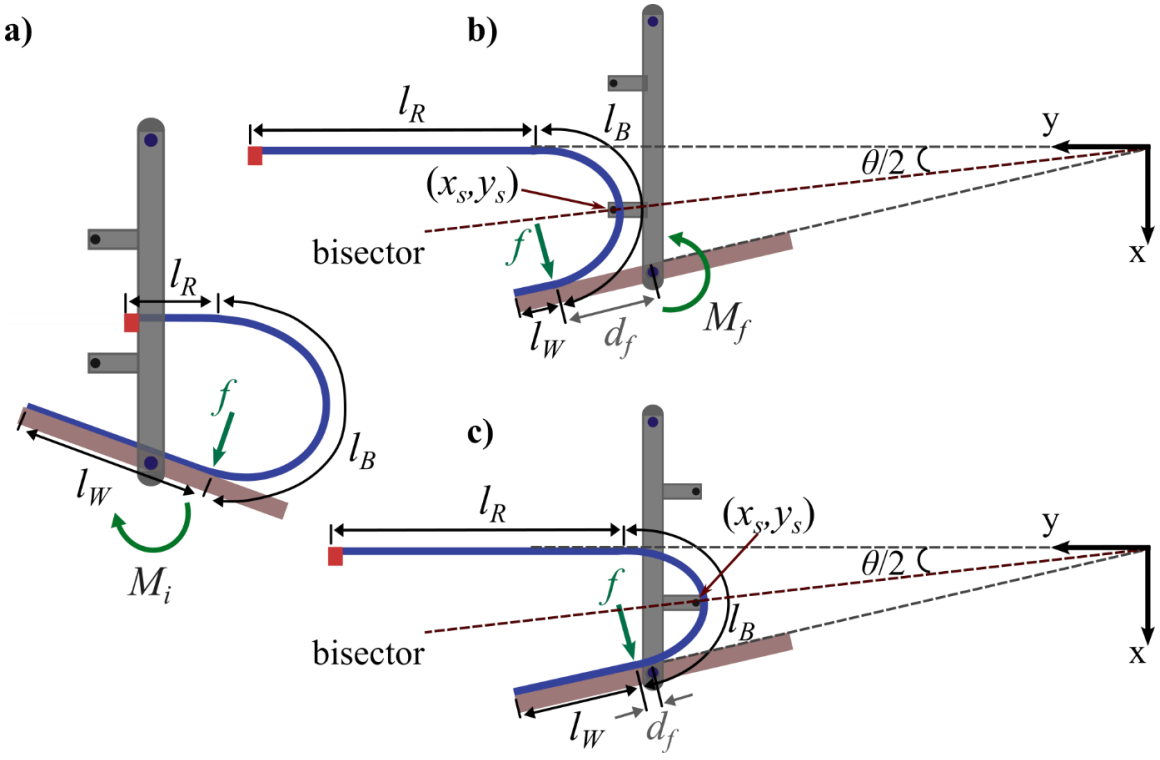

Figure S 26. Geometrical parameters of the strip including different length sections and force and moment in one bistable cell at a) initial configuration, and b-c) final configuration.

As Figure S26b-c suggests, the axial stopper can be positioned on either the right side or the left side of the hinge. It is important to notice that the moment capacity M_f depends on both contact force f and moment arm d_f, since $M_f = f.d_f$. Having the stopper on the left side means a larger moment arm, while contact force is smaller and on the right side it is vice versa. Therefore, choosing the right point for the axial stopper is a value optimization problem that depends on the variation of contact force with displacement.

The activation force (F_a) profile is obtained from the tensile test (Figure S27) performed on the activation tendon with 10 mm/s speed. After less than 1 second loading up to 3.3 N load, two segments snapped within 110 ms and then, third segment snapped in 80 ms after less than 4 seconds of loading up to 4.5 N. The zero force between the first and second snap is because the activation tendon becomes slack after first snap and doesn't have any resistance force until before t = 3.7 s.

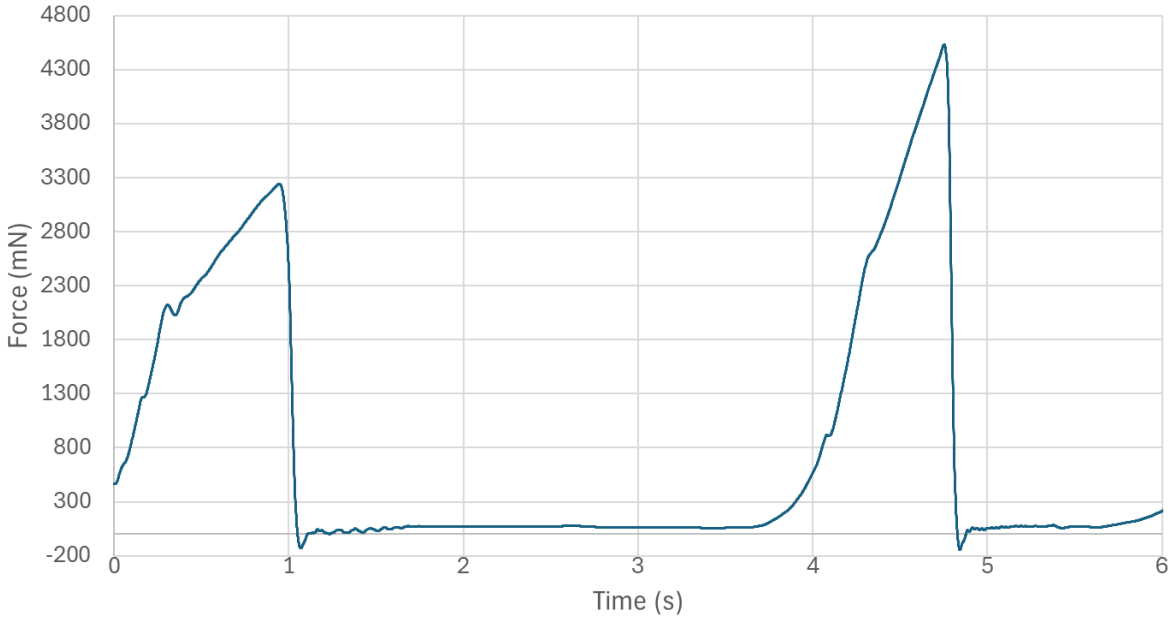

Figure S 27- Activation force of the three segment gripper data measured using tensile test machine.

SI-9. Codes

SI-9.1. Inverse problem with known eccentricity, *ecc*.

Ellipse fitting code in MATLAB to solve the inverse problem of cases 1 and 2 and plotting the results. In this condition, the eccentricity (*ecc*) for a specific angle is known and is used as an input. Therefore, we can compute the value of different length sections of the strip for the given input values of geometry. Explanations are included in code.

```
function Ellipse_fitting
%% Ellipse fitting
% Condition 1: Known tangency point on inclined wall (y=mx). Major axis & center on bisector.
% Condition 2: Known horizontal tangent line y = P_jy + l_d*cos(theta). Major axis & center on bisector; also tangent to x=0.
% For both, compute short/long ellipse arcs between the two corresponding tangency points.
% Outputs:
%   "Condition 1 (convergent section): l_B = '<Lshort1>'"
%   "Condition 2 (divergent section): l_B = '<Llong2>' and l_w = '<lc + d_p>'"
% Notes: d_p is used ONLY in Condition 2 output;

clear; clc; close all

%% -------------------- Inputs --------------------
W       = 70.0;          % width parameter
theta   = deg2rad(25);   % radians
 ecc_c  = 0.7298;        % Condition 1 eccentricity (0<=ecc_c<1)
 ecc_d  = 0.6824;        % Condition 2 eccentricity (0<=ecc_d<1)
lc      = 42.5;          % long-segment top offset from P_j
ld      = 50;            % long-segment bottom offset from P_j
 e_wall = 2.5;           % short T-segment length (the wall eccentricity, 'e')
lw      = 10;            % (COND 1 only) offset from P_T down to the tangency point along wall
plot_margin = 50.0;

%% -------------------- Lines and orientation --------------------
% Inclined wall: y = m x with m = cot(theta)
m  = cot(theta);
% Angle-bisector: y = mp x with mp = cot(theta/2)
mp = cot(theta/2);
% Orientation of ellipse major axis (fixed)
alpha = atan(mp);

R  = [cos(alpha) -sin(alpha); sin(alpha) cos(alpha)];
RT = R.';

%% -------------------- Build T-shaped inclined wall --------------------
% Short segment free endpoint P_r
Prx =  W/2;
Pry = (W*cos(theta) - 2*e_wall)/(2*sin(theta));
Pr  = [Prx; Pry];

% Short-long junction P_j
Pjx = Prx - e_wall*cos(theta);
Pjy = Pry + e_wall*sin(theta);
Pj  = [Pjx; Pjy];

% Long segment endpoints P_B (bottom) and P_T (top)
PBx = Pjx - ld*sin(theta);
PBy = Pjy - ld*cos(theta);
PB  = [PBx; PBy];

PTx = Pjx + lc*sin(theta);
PTy = Pjy + lc*cos(theta);
PT  = [PTx; PTy];

% Horizontal tangent line for CONDITION 2
y_h = Pjy + ld*cos(theta);   % y = y_h
```

```
%% -------------------- CONDITION 1: tangency point on inclined wall --------------------
% Specified tangency point on the long segment
xt = PTx - lw*sin(theta);
yt = PTy - lw*cos(theta);
Pt1 = [xt; yt];

% Wall normal and its BODY-frame version
n_incline = [-m; 1]; n_incline = n_incline/norm(n_incline);
w = RT * n_incline;  % (w1,w2)

% Solve for [a1; h1] with center constrained to bisector (k1 = mp*h1)
[a1,h1] = solve_cond1(Pt1, R, RT, w, mp, ecc_c);
k1 = mp*h1; b1 = a1*sqrt(1 - ecc_c^2); c1 = [h1; k1];

% Second tangency (to x=0) via symmetry/mirror across the bisector
u = R(:,1);                    % unit dir of bisector
p_vert1 = 2*u*(u.'*Pt1) - Pt1;  % mirror of Pt1

% Arc parameters for Condition 1
[t1a, t1b] = ellipse_params_at_points(Pt1, p_vert1, c1, a1, b1, RT);
[Lshort1, Llong1, XYw1, tt1, idxShort1, idxLong1] = arc_lengths_and_paths(a1,b1,t1a,t1b,R,c1);

%% -------------------- CONDITION 2: tangent to x=0 and to horizontal y=y_h --------------------
% Here we solve for a2,h2 so that:
%   (i) tangency to x=0 -> -h + rho_x = 0 (use left-facing normal [-1;0])
%   (ii) tangency to y=y_h (assume upper) -> k + rho_y = y_h, with k=mp*h
% Unknowns: [a; h]. b follows from ecc_d.

[a2,h2] = solve_cond2(y_h, R, RT, mp, ecc_d);
k2 = mp*h2; b2 = a2*sqrt(1 - ecc_d^2); c2 = [h2; k2];

% Tangency points for Condition 2
% Enforce endpoints as true contacts with the two walls:
%   - vertical wall x=0 : normal n_x = [-1; 0]  => ensures x=0
%   - inclined wall y=mx: obtained by MIRROR of pt_x0_2 across bisector (guarantees symmetry & line alignment)
n_x = [-1;0];           % left-facing normal for x=0
n_y = [0;1];            % +y (upper horizontal line, used for fitting & reference)
pt_x0_2 = contact_point_world(c2, a2, b2, R, RT, n_x);       % tangency on x=0 (enforced)
% Mirror across bisector to get inclined-wall tangency
u = R(:,1);                          % unit dir along bisector
pt_mx_2 = 2*u*(u.'*pt_x0_2) - pt_x0_2;   % tangency on y = m x (by symmetry)
% Reference horizontal contact (not used for arcs)
pt_h_2  = contact_point_world(c2, a2, b2, R, RT, n_y);

% Arc parameters for Condition 2 (between inclined-wall and vertical-wall tangencies)
[t2a, t2b] = ellipse_params_at_points(pt_mx_2, pt_x0_2, c2, a2, b2, RT);
[Lshort2, Llong2, XYw2, tt2, idxShort2, idxLong2] = arc_lengths_and_paths(a2,b2,t2a,t2b,R,c2);

% d_p is distance from P_j to the Condition 1 tangency along the wall dir,
% used only to report l_w for Condition 2 as l_c + d_p
wall_dir = [sin(theta); cos(theta)];  % unit along the wall
 d_p = dot(Pt1 - Pj, wall_dir);
lw_cond2 = lc + d_p;

%% -------------------- PLOTS --------------------
% Condition 1 plot
figure('Color','w'); hold on; axis equal;
allPts1 = [Pr, Pj, PB, PT, Pt1, p_vert1, c1];
xmin = min(allPts1(1,:)) - plot_margin; xmax = max(allPts1(1,:)) + plot_margin;
ymin = min(allPts1(2,:)) - plot_margin; ymax = max(allPts1(2,:)) + plot_margin;

plot([0 0],[ymin ymax],'k--','LineWidth',1.5,'DisplayName','x = 0');
xx = linspace(xmin, xmax, 2);
plot(xx, m*xx, 'k-.','LineWidth',1.5,'DisplayName','y = m x');
plot(xx, mp*xx, 'g--','LineWidth',1.2,'DisplayName','bisector');
plot([Pr(1) Pj(1)],[Pr(2) Pj(2)],'-','Color',[0.65 0.25 0.25],'LineWidth',4,'DisplayName','Short segment');
plot([PB(1) PT(1)],[PB(2) PT(2)],'-','Color',[0.25 0.25 0.75],'LineWidth',4,'DisplayName','Long segment');

% Ellipse
```

```
plot(XYw1(1,:), XYw1(2,:), 'k', 'LineWidth',2, 'DisplayName','Ellipse (C1)');
plot(Pt1(1), Pt1(2), 'ro', 'MarkerFaceColor','r', 'DisplayName','Tangency on y=mx');
plot(p_vert1(1), p_vert1(2), 'mo', 'MarkerFaceColor','m', 'DisplayName','Tangency on x=0');

% Arcs
plot(XYw1(1,idxShort1), XYw1(2,idxShort1), 'r--','LineWidth',3,'DisplayName',sprintf('Short arc (%.6f)', Lshort1));
plot(XYw1(1,idxLong1),  XYw1(2,idxLong1),  'c--','LineWidth',2,'DisplayName',sprintf('Long arc (%.6f)',  Llong1));

plot(c1(1), c1(2), 'ks','MarkerSize',8,'MarkerFaceColor','k','DisplayName','Center');
legend('Location','bestoutside'); grid on;
xlim([xmin xmax]); ylim([ymin ymax]);
xlabel('X'); ylabel('Y'); title('Condition 1');

% Condition 2 plot
figure('Color','w'); hold on; axis equal;
allPts2 = [Pr, Pj, PB, PT, pt_x0_2, pt_mx_2, c2];
xmin = min(allPts2(1,:)) - plot_margin; xmax = max(allPts2(1,:)) + plot_margin;
ymin = min(allPts2(2,:)) - plot_margin; ymax = max(allPts2(2,:)) + plot_margin;
plot([0 0],[ymin ymax],'k--','LineWidth',1.5,'DisplayName','x = 0');
xx = linspace(xmin, xmax, 2);
plot(xx, mp*xx, 'g--','LineWidth',1.2,'DisplayName','bisector');
plot(xx, m*xx, 'k-.','LineWidth',1.5,'DisplayName','y = m x');

% Horizontal tangent line
plot([xmin xmax], [y_h y_h], 'b:', 'LineWidth',2, 'DisplayName', sprintf('y = P_{jy} + l_d cos(\\theta) = %.4f', y_h));

% Ellipse
plot(XYw2(1,:), XYw2(2,:), 'k', 'LineWidth',2, 'DisplayName','Ellipse (C2)');
plot(pt_mx_2(1), pt_mx_2(2), 'ro', 'MarkerFaceColor','r', 'DisplayName','Tangency on y=mx');
plot(pt_x0_2(1), pt_x0_2(2), 'mo', 'MarkerFaceColor','m', 'DisplayName','Tangency on x=0');
plot(pt_h_2(1),  pt_h_2(2),  'bo', 'MarkerFaceColor','b', 'DisplayName','Tangency on y=y_h (ref)');

% Arcs
plot(XYw2(1,idxShort2), XYw2(2,idxShort2), 'r--','LineWidth',3,'DisplayName',sprintf('Short arc (%.6f)', Lshort2));
plot(XYw2(1,idxLong2),  XYw2(2,idxLong2),  'c--','LineWidth',2,'DisplayName',sprintf('Long arc (%.6f)',  Llong2));

plot(c2(1), c2(2), 'ks','MarkerSize',8,'MarkerFaceColor','k','DisplayName','Center');
legend('Location','bestoutside'); grid on;
xlim([xmin xmax]); ylim([ymin ymax]);
xlabel('X'); ylabel('Y'); title('Condition 2');

%% ---------- Textual outputs ----------
fprintf('Condition 1 (convergent section): l_B = "%.9f"', Lshort1);
fprintf('Condition 2 (divergent section): l_B = "%.9f" and l_w = "%.9f"', Llong2, lw_cond2);

end % <-- end main function
%% ---------- Helper fns ----------
function [a,h] = solve_cond1(Pt, R, RT, w, mp, ecc_c)
    % Two equations in two unknowns: a, h; center k=mp*h; b=a*sqrt(1-ecc_c^2)
    h0 = max(1.0, abs(Pt(1))); a0 = max(1.0, norm(Pt));
    % pick sign to stabilize
    b0 = a0*sqrt(1-ecc_c^2);
    q0 = RT * (Pt - [h0; mp*h0]);
    S0 = sqrt( (w(1)^2)*a0^2 + (w(2)^2)*b0^2 );
    r0 = [ (a0^2)*w(1) ; (b0^2)*w(2) ] / S0; sgn = 1; if dot(q0,r0)<0, sgn = -1; end
    F = @(x) residual_twoeq_c(x, Pt, R, RT, sgn*w, mp, ecc_c);
    opts = optimoptions('fsolve','Display','off','FunctionTolerance',1e-12,'StepTolerance',1e-12,'OptimalityTolerance',1e-12);
    xsol = fsolve(F, [a0; h0], opts);
    a = xsol(1); h = xsol(2);
end

function [a,h] = solve_cond2(y_h, R, RT, mp, ecc_d)
    % Solve for tangency to x=0 and to y=y_h with center on bisector
    n_x = [-1;0]; n_y = [0;1];  % IMPORTANT: use left normal for x=0 so -h + rho = 0
    u = R(:,1); v = R(:,2);
    rho = @(a,bb,n) 1 ./ sqrt( ( (dot(n,u)^2) ./ a.^2 ) + ( (dot(n,v)^2) ./ bb.^2 ) );
    F = @(x) cond2_residual(x, rho, n_x, n_y, mp, y_h, ecc_d);
    % Initial guess from Condition 1 style scale
    a0 = max(1.0, abs(y_h)); h0 = max(1.0, 0.5*a0);
    opts = optimoptions('fsolve','Display','off','FunctionTolerance',1e-12,'StepTolerance',1e-12,'OptimalityTolerance',1e-12);
```

```
    xsol = fsolve(F, [a0; h0], opts);
    a = xsol(1); h = xsol(2);
end

function F = cond2_residual(x, rho, n_x, n_y, mp, y_h, ecc_d)
    a = x(1); h = x(2); if a<=0, F=[1;1]*1e3; return; end
    b = a*sqrt(1 - ecc_d^2); k = mp*h;
    rho_x = rho(a,b,n_x);
    rho_y = rho(a,b,n_y);
    % (i) -h + rho_x = 0  (tangent to x=0 with left normal)
    F1 = -h + rho_x;
    % (ii)  k + rho_y = y_h (upper horizontal tangent)
    F2 = k + rho_y - y_h;
    F = [F1; F2];
end

function [tA, tB] = ellipse_params_at_points(PA, PB, c, a, b, RT)
    XY_A = RT*(PA - c); XY_B = RT*(PB - c);
    tA = mod(atan2(XY_A(2)/b, XY_A(1)/a), 2*pi);
    tB = mod(atan2(XY_B(2)/b, XY_B(1)/a), 2*pi);
end

function [Lshort, Llong, XYw, tt, idxShort, idxLong] = arc_lengths_and_paths(a,b,t1,t2,R,c)
    spd = @(u) sqrt( a^2.*sin(u).^2 + b^2.*cos(u).^2 );
    C   = integral(spd, 0, 2*pi, 'AbsTol',1e-12,'RelTol',1e-10);
    arc_between = @(s,t) ( (t>=s).*integral(spd,s,t,'AbsTol',1e-12,'RelTol',1e-10) + ...
                           (t< s).*(integral(spd,s,2*pi,'AbsTol',1e-12,'RelTol',1e-10) + ...
                                    integral(spd,0,t,'AbsTol',1e-12,'RelTol',1e-10)) );
    L12    = arc_between(t1,t2); Lshort = min(L12, C-L12); Llong = C - Lshort;
    % polyline sampling and index split
    tt  = linspace(0,2*pi,1600);
    XY  = [a*cos(tt); b*sin(tt)]; XYw = R*XY + c;
    wrap = @(ang) mod(ang, 2*pi);
    [~, i1] = min(abs(wrap(tt) - t1));
    [~, i2] = min(abs(wrap(tt) - t2));
    if i1 <= i2
        idxA = i1:i2;               % direct path
        idxB = [i2:length(tt), 1:i1]; % wrap path
    else
        idxA = [i1:length(tt), 1:i2]; % wrap path
        idxB = i2:i1;               % direct path reversed
    end
    lenA = sum(vecnorm(diff(XYw(:,idxA),1,2),2,1));
    lenB = sum(vecnorm(diff(XYw(:,idxB),1,2),2,1));
    if lenA <= lenB
        idxShort = idxA; idxLong = idxB;
    else
        idxShort = idxB; idxLong = idxA;
    end
end

function p = contact_point_world(c, a, b, R, RT, n)
    n_local = RT * n;
    den     = sqrt( (a*n_local(1))^2 + (b*n_local(2))^2 );
    Xc      = (a^2) * n_local(1) / den;
    Yc      = (b^2) * n_local(2) / den;
    p       = c + R * [Xc; Yc];
end

function F = residual_twoeq_c(x, Pt, R, RT, w, mp, ecc_c)
    % Two equations in two unknowns for Condition 1 (ecc_c): a, h (center on bisector)
    a  = x(1); h = x(2);
    if a<=0, F = [1e3;1e3]; return; end
    b  = a*sqrt(1 - ecc_c^2);
    c  = [h; mp*h];
    q  = RT * (Pt - c);                     % body coords of target point
    S  = sqrt( (w(1)^2)*a^2 + (w(2)^2)*b^2 );   % normalization
    r  = [ (a^2)*w(1) ; (b^2)*w(2) ] / S;       % required body vector at tangency
    F  = q - r;                             % enforce point & slope tangency
end
```

SI-9.2. Finding stress and strain using inverse problem of ellipse fitting

This code derives the maximum stress knowing the thickness of strip *t* and elastic modulus *E*. Inputs are provided to check as an example inside the function. This function could be called for value optimization in another code to find the right values of parameters to maximize strain and minimize stress or another single or multi-objective optimization.

```
function [sigma_max1, sigma_max2, kappa_max1, kappa_max2, a1, a2, b1, b2, l_s, l_R2, l_B2, l_w2, l_R1, l_B1, epsilon] = Stress_Strain(W, theta_deg, ecc_c, ecc_d, lc, ld, e_wall, lw, E, t)
%STRESS_STRAIN Compute stress/strain and strip length metrics from fitted ellipses.
%
% Uses Ellipse_fitting for geometry; no plots here.
%
% Inputs (geometry): W, theta_deg, ecc_c, ecc_d, lc, ld, e_wall, lw
% Inputs (material): E (Young's modulus), t (thickness)
%
% Outputs (existing):
%   sigma_max1, sigma_max2 - max bending stress at max curvature (Cond 1,2)
%   kappa_max1, kappa_max2 - max curvature (Cond 1,2)
%   a1, a2                 - major semi-axes (Cond 1,2)
%   b1, b2                 - minor semi-axes (Cond 1,2)
% New outputs:
%   l_s                    - strip length (constant between conditions)
%   l_R2, l_B2, l_w2       - rolling, arc, and wall lengths for Condition 2
%   l_R1, l_B1             - rolling and arc for Condition 1 (with l_w1 = 0)
%   epsilon                - strain defined per user formula
%
% Requires Ellipse_fitting.m on path.

% Inputs
W       = 70.0;         % width parameter
theta_deg   = 25;   % radians
ecc_c  = 0.7298;       % Condition 1 eccentricity (0<=ecc_c<1)
ecc_d  = 0.6824;       % Condition 2 eccentricity (0<=ecc_d<1)
lc      = 42.5;         % long-segment top offset from P_j
ld      = 50;           % long-segment bottom offset from P_j
e_wall = 2.5;          % short T-segment length (the 'e')
lw      = lc;
E = 210000;
t = 0.2;

%% --- Call function with provided lw (general case) ---
[Lshort1_cur, Llong1_cur, Lshort2, Llong2, lw_cond2, a1, a2] = ...
    Ellipse_fitting (W, theta_deg, ecc_c, ecc_d, lc, ld, e_wall, lw);

% Minor semi-axes
b1 = a1 * sqrt(1 - ecc_c^2);
b2 = a2 * sqrt(1 - ecc_d^2);

% Max curvature (rotation-invariant) and bending stress
kappa_max1 = a1 / (b1^2);
kappa_max2 = a2 / (b2^2);
sigma_max1 = E * kappa_max1 * (t/2);
sigma_max2 = E * kappa_max2 * (t/2);

%% ================= Condition 2 strip length (defines l_s) =================
% Geometry needed (P_T, bisector orientation, etc.)
theta    = deg2rad(theta_deg);
mp       = cot(theta/2);
alpha    = atan(mp);
R        = [cos(alpha) -sin(alpha); sin(alpha) cos(alpha)];
RT       = R.';
```

```
% Key points to compute P_T (top of long segment)
Prx =  W/2;
Pry = (W*cos(theta) - 2*e_wall)/(2*sin(theta));
Pjx = Prx - e_wall*cos(theta);
Pjy = Pry + e_wall*sin(theta);
PTx = Pjx + lc*sin(theta);
PTy = Pjy + lc*cos(theta);
PT  = [PTx; PTy]; %#ok<NASGU>

% Recover center for Condition 2 to get actual tangency point on x=0
b2_local = b2;
nx = [-1;0];                % vertical wall outward normal (left-facing)
u  = R(:,1);                % bisector dir (not needed for this y, but handy)
% From cond2 solver relation: -h + rho_x = 0 => h = rho_x
rho_x = 1 / sqrt( ( (dot(nx, R(:,1))^2) / a2^2 ) + ( (dot(nx, R(:,2))^2) / b2_local^2 ) );
h2    = rho_x;
k2    = mp*h2;
c2    = [h2; k2];
pt_x0_2 = contact_point_world(c2, a2, b2_local, R, RT, nx);

% Length components for Condition 2
l_B2 = Llong2;       % per spec: use long arc in divergent section
l_w2 = lw_cond2;     % from v3
l_R2 = abs(PTy - pt_x0_2(2));  % vertical distance between P_T and x=0 tangency

% Strip length (constant)
l_s  = l_R2 + l_B2 + l_w2;

%% ================== Condition 1 with l_w1 = 0 ==================
% Re-evaluate condition 1 with l_w1 = 0 to get l_B1 and vertical tangency
lw1  = 0;
[Lshort1_0, ~, ~, ~, ~, a1_0] = Ellipse_fitting (W, theta_deg, ecc_c, ecc_d, lc, ld, e_wall, lw1); %#ok<ASGLU>
l_B1 = Lshort1_0;    % per spec: use short arc in convergent section

% Tangency point on x=0 for Cond 1 when lw1 = 0: mirror of P_T across bisector
Pt1_0    = [PTx; PTy];
u        = R(:,1);
p_vert1_0 = 2*u*(u.'*Pt1_0) - Pt1_0;
yt_x0_1   = p_vert1_0(2);   % y-coordinate of vertical-wall tangency (Cond 1)

% l_R1 from strip length constraint
l_w1 = 0;
l_R1 = l_s - (l_B1 + l_w1);

% Define L and strain epsilon per user formula
L = l_R1 + yt_x0_1 - Pry;
epsilon = (l_R1 + yt_x0_1 - PTy) / L;

% (Optional) print a concise summary
fprintf('l_s = %.6f | C2: l_R2 = %.6f, l_B2 = %.6f, l_w2 = %.6f', l_s, l_R2, l_B2, l_w2);
fprintf('C1 (lw1=0): l_R1 = %.6f, l_B1 = %.6f, yt(x=0) = %.6f, epsilon = %.6e', l_R1, l_B1, yt_x0_1, epsilon);

end

%% ---- Local helper (copy from v3 for contact point) ----
function p = contact_point_world(c, a, b, R, RT, n)
   n_local = RT * n;
   den     = sqrt( (a*n_local(1))^2 + (b*n_local(2))^2 );
   Xc      = (a^2) * n_local(1) / den;
   Yc      = (b^2) * n_local(2) / den;
   p       = c + R * [Xc; Yc];
end
```

References

[1] Iwamoto, Takaya. *The effect of end fixity on the stability of structures*. Diss. Georgia Institute of Technology, 1970.

[2] De Domenico, D., G. Falsone, and D. Settineri. "Probabilistic buckling analysis of beam-column elements with geometric imperfections and various boundary conditions." *Meccanica* 53.4 (2018): 1001-1013.

[3] Gisby, Todd A., Benjamin M. O'Brien, and Iain A. Anderson. "Self sensing feedback for dielectric elastomer actuators." *Applied Physics Letters* 102.19 (2013).

[4] Rosset, Samuel, et al. "Self-sensing dielectric elastomer actuators in closed-loop operation." *Smart Materials and Structures* 22.10 (2013): 104018.

[5] Bluett, Simon, et al. "Self-sensing electro-ribbon actuators." *IEEE robotics and automation letters* 5.3 (2020): 3931-3936.